Dottorato di ricerca in FISICA
UNIVERSITà DEGLI STUDI DI PARMA
XXII ciclo

Coordinatore : Prof. Antonio Deriu

Structure and dynamics of bio-hydrogels investigated by neutron and X-ray scattering techniques

---

Dottoranda: Chiara CHIAPPONI
Relatore: Prof. Antonio DERIU

Parma, Italia, 2010

Ringraziamenti

Grazie al Professor Deriu per tutto quello che mi ha insegnato. Grazie a Maria Teresa per i preziosi consigli di programmazione. Grazie a Ivana Finelli e al Professor Paradossi per la chimica. Grazie a Laura Cantù per le sedute di basso angolo e le iniezioni di autostima. Grazie a Francesca Natali per il periodo Grenoblese.

Riassunto

L'acido ialuronico (HYA) è un polisaccaride naturale, appartenente alla famiglia dei glicosaminoglicani, caratterizzato dalla ripetizione di un' unità disaccaridica composta da acido glucuronico ed N-acetilglucosammina. Lo HYA è presente in tutto il regno animale, dalle matrici extracellulari in cui molti tessuti si differenziano, all'umor vitreo dell'occhio umano, al fluido sinoviale in corrispondenza delle giunture. Grazie alla sua abilità di formare soluzioni viscose in acqua, lo HYA è ampiamente impiegato nei trattamenti delle malattie infiammatorie e degenerative delle articolazioni, un gruppo di patologie con elevato impatto sociale in quanto fortemente legate all'aumento dei costi sanitari ed alla qualità della vita.

Dell'acido ialuronico abbiamo studiato anche una forma chimicamente modificata, lo HYADD, ottenuta derivatizzando, attraverso legami ammidici, la catena principale del polisaccaride con catene laterali esadeciliche (C-16) con un grado di sostituzione dell'1-3% delle unità ripetitive. La modifica, pur essendo piccola, altera drammaticamente alcune delle proprietà macroscopiche come il comportamento elastico e la riposta reologica del polimero. Con lo HYADD si ottiene un idrogel relativamente stabile a concentrazioni polimeriche superiori allo 0.3% (peso polimero/ volume totale), mentre l'acido ialuronico naturale forma soluzioni viscose a concentrazioni dieci volte superiori. Lo HYADD, tuttavia, non differisce dallo HYA in altre caratteristiche importanti quali la densità di carica lungo

la catena, l'abilità di 'swelling' o il comportamento d'interazione con metaboliti e materiale cellulare nella matrice sinoviale. Sulla base degli effetti benefici notati in recenti test condotti su modelli animali di osteoartrite, si pensa che lo HYADD possa avere effetti clinici positivi nella mobilità e nella funzione delle articolazioni.

Lo scopo principale di questa tesi è quello di confrontare il gel naturale e quello chimicamente modificato sulla base di proprietà strutturali quali l'organizzazione delle catene polimeriche e di proprietà dinamiche come la micro diffusività dell'acqua nel gel. Per studiare i due sistemi polimerici in diverse condizioni di temperatura e concentrazione, abbiamo condotto diversi esperimenti di scattering di raggi X e neutroni. Dal punto di vista strutturale abbiamo scoperto che lo HYADD ha una struttura più compatta dello HYA, dovuta ai bracci laterali presenti lungo la catena principale. Le lunghezze caratteristiche ($\sim$150 Å) derivate dagli esperimenti di neutroni e raggi X, sono in buon accordo con quelle risultanti dalle misure di scattering dinamico della luce. Sui gels più concentrati, inoltre, i patterns di diffrazione a basso angolo mostrano la presenza di qualche grado d'ordine nell'organizzazione della catena saccaridica di HYA. La dinamica delle catene di HYA e HYADD mostra alcune piccole differenze sulla scala temporale tra i 100 e i 1000 ps (principalmente nella regione a bassi Q), che può essere collegata alla presenza della modifica chimica. La dinamica diffusiva dell'acqua nel gel invece risulta simile a quella dell'acqua bulk sia per lo HYA che per lo HYADD, almeno fino ad una concentrazione del 10%.

Nel contesto di una collaborazione col gruppo della Prof.ssa Santi del Dipartimento di Farmacia dell'Università di Parma, abbiamo contribuito alla caratterizzazione di una nuova piattaforma chiamata Patch-non Patch, sviluppata per il trasporto transdermico del farmaco. In particolare, abbiamo studiato la diffusività di un farmaco modello (lidocaina) attraverso il

cerotto con lo scattering quasi-elastico di neutroni. I dati ottenuti indicano che la diffusione della lidocaina è triggerata da quella dell'acqua di idratazione presente nel cerotto.

Grazie al finanziamento del CNR, ho potuto trascorrere 18 mesi all' Institut Laue Langevin a Grenoble, ospite del gruppo di ricercatori italo-francesi responsabili dello spettrometro a retrodiffusione IN13. Sotto la supervisione della Dott.ssa Francesca Natali, ho partecipato alle attività del gruppo, contribuendo ad esempio agli sviluppi tecnici e all'assistenza degli utilizzatori durante gli esperimenti.

Abstract

Hyaluronic acid (HYA) is a natural polysaccharide, belonging to the family of glycosaminoglycans, characterized by the repetition of a disaccharide unit of glucuronic acid and N-acetylglucosamine. HYA is present throughout the animal kingdom, from the extracellular matrices in which most tissues differentiate, to the vitreous of the human eye and the synovial joint fluid. Thanks to its ability to form viscous solutions in water, HYA is widely used to treat inflammatory and degenerative joint diseases, a group of pathologies with a high impact in society since they contribute heavily to the rise of health costs and they affect life quality. Beside HYA, we investigated a chemically modified form of hyaluronic acid, HYADD, obtained derivatizing the polysaccharide backbone with hexadecylic (C-16) side chains, through amide bonds, with a 1-3 mol-% degree of substitution of repeating units. Even if the modification is very small, it alters dramatically some macroscopic properties such as the elastic behavior and the rheological response. The resulting system is a relatively stable hydrogel at polymer concentrations higher than 0.3% (weight of polymer/total volume), whereas native hyaluronic acid forms highly viscous solutions only at concentrations ten times higher. HYADD, however, does not differ from HYA in other relevant features such as charge density along the chain and swelling ability, as well as in its interaction behavior with metabolites and cellular material in the synovial matrix. On the basis of the beneficial

effects noticed in recent tests performed on animal models of osteoarthritis, HYADD is expected to have a positive clinical effect in joint mobility and function.

The aim of this PhD thesis is to compare the natural gel and the chemically modified one focusing on microscopic structural and dynamic properties such as the structure and organization of the polymer chains, the dynamics of the polymer and the self-diffusivity of water in the gels. We have performed several experiments using X-ray and neutron scattering to probe gels at different polymer concentrations and temperatures. From the structural point of view we found that HYADD has a structure more compact than HYA owing to the hexadecylic branches added along the chain. The characteristic lengths derived from neutron and X-ray experiments ($\sim$150 Å) are in fair agreement with those resulting from dynamics light scattering measurements. The small angle diffraction patterns show, in addition, the presence of some degree of order in the organization of the natural saccharide chain in the most concentrated gels. The dynamics of HYA and HYADD shows some small differences in the 100-1000 ps timescale (mostly in the low-Q region) that can be related to the presence of the chemical modification. On the other hand the diffusive dynamics of gel water is similar to that of bulk water for both HYA and HYADD gels at least up to 10% gel concentration.

In the frame of a collaboration with the group of Prof. Santi at the Department of Pharmacy of Parma University, we contributed to the characterization of a novel platform called Patch-non Patch®, developed for transdermal drug delivery. In particular, using quasielastic neutron scattering we investigated the diffusivity of a model drug (lidocaine) through the patch. The obtained data indicate that the diffusion of lidocaine is triggered by that of hydration water present in the patch.

In the framework of a CNR PhD grant, I spent 18 months at the Institut

Laue Langevin in Grenoble, where I joined the group of Italian and French researchers in charge of the backscattering spectrometer IN13. Under the supervision of Dr. Francesca Natali, I took part to the group activities, contributing to the technical developments and to the assistance to users during their experiments.

Contents

1 Introduction **1**

2 Radiations to probe soft matter **8**

2.1 How to probe dynamical processes 8

2.2 Structural investigation 14

2.3 Performing a real experiment 18

3 The backscattering spectrometer IN13 **19**

3.1 Functioning of a backscattering spectrometer 19

3.2 Being part of IN13 team 23

4 Hyaluronic acid gels **32**

4.1 Gel preparation 34

4.2 Structure of the polymer chains 35

4.2.1 Small angle diffractometers 35

4.2.2 Data analysis 37

4.2.3 Results and discussion 39

4.3 Polymer dynamics 46

4.3.1 Elastic and quasi-elastic scattering experiments . . . 46

4.3.2 Data analysis and results 47

4.4 Dynamics of water 55

4.4.1 QENS experiment 55

4.4.2 Data analysis 56
4.4.3 Results and discussion 59
4.5 Conclusions 62

5 Transdermal patches **65**
5.1 Experimental 66
5.1.1 Sample preparation 66
5.1.2 QENS experiment 68
5.2 Data analysis 69
5.3 Results and discussions 73
5.3.1 Dynamics of empty patches 74
5.3.2 Dynamics of hydration water 78
5.3.3 Dynamics of Lidocaine 78
5.4 Conclusions 83

Chapter 1

Introduction

The main topic of this thesis is the investigation of structure and dynamics of polysaccharide hydrogels performed using neutrons and X-rays scattering techniques. In the last decades, gels have become the object of many researches in physics, chemistry, material science and so on. A gel is formed when a polymeric system undergoes to specific conditions of temperature, pressure, concentration or when an external agent is inserted to make links between the molecules: in such situations a network of flexible chains is created. Gels occupy an intermediate position between a free solution of macromolecules and a porous solid: morphological variations are inhibited and the translational motions of the polymer main chain are frozen. A gel is a network in which the meshes of the net are filled with a solvent which may diffuse between the meshes and inside them; moreover it may eventually interact with the polymer chains. In this thesis the specific systems considered are hydrogels, i.e. gels in which the solvent is water.

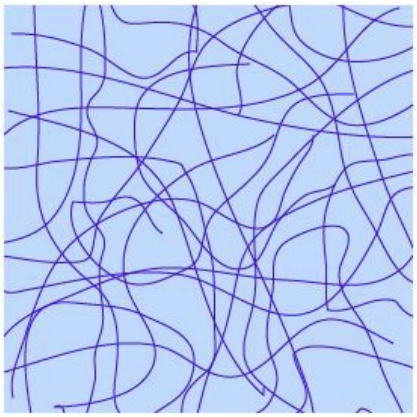

Figure 1.1: Sketch of a gel structure: a net of long molecules similar to ribbons that are somehow (physically or chemically) linked up.

The formation of a gel can derive both from physical and chemical processes. Since the final properties of the system may depend significantly on the way of preparation, it is worth giving a brief description:

- A *chemical gel*, also called *strong* or *irreversible* gel, is the result of a gelation process made through chemical methods starting from a liquid phase. Using techniques such as polycondensation or additive polymerization, covalent bonds are induced between molecules: the new phase is rather stable and the system can be considered in equilibrium until extreme conditions occur and degrade the network. For a chemical gel, the *sol-gel* transition is sharp and it corresponds to an instantaneous switch between a liquid phase and an infinite aggregate.

- A *physical gel*, also called *weak* or *reversible* gel, is obtained applying a physical process able to induce the association between particles originally in the liquid phase. The links formed in these conditions are very unstable: they can brake under the action of a finite stress

and reform again once the perturbation is finished. The thermal history of a physical gel is therefore very important to understand its properties.

This thesis will present the analysis carried out on hydrogels based on hyaluronic acid developed during my PhD. Hyaluronic acid, hereafter called HYA, is a natural polysaccharide present throughout the animal kingdom and belonging to the family of glycosaminoglycans; it is characterized by the repetition of the disaccharide unit shown in Figure 1.2. The monomer has length ~ 10 Å and weight 400 g/mol.

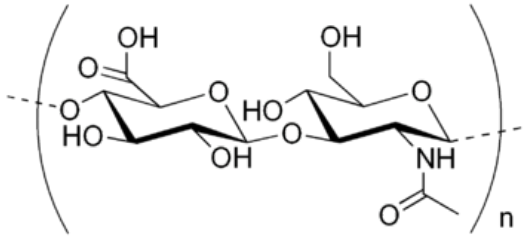

Figure 1.2: Monomeric unit of hyaluronic acid chain

HYA is present in every tissue of human body and it performs many important functions: it helps for instance the delivery of nutrients to, and the transport of toxins from cells that do not have a blood supply, such as those found in cartilage; an adequate amounts of HYA keeps joints lubricated, avoiding their deterioration. In certain tissues of the body it also encourages water retention. Large concentrations of HYA are found in the extracellular matrix, the fluid-filled space between cells: there, HYA function is to lock moisture into the matrix, to keep collagen and elastin humid, preventing cellular aging. Nowadays HYA is widely used by cosmetic and medical industries. The medical applications span from ophthalmic treatments to injections to heal rheumatism and osteoarthrosis. For the latter in particular, chemically modified forms of HYA are becoming more

and more used. The specific modified species hereafter treated is called HYADD4^{TM} (in the following just HYADD): it is obtained derivatizing the polysaccharidic backbone of HYA with side chains of 16 carbonium atoms (hexadecylic chains) grafted through amide bonds; the degree of substitution is only $1 - 3$ % of the repeating units (see Figure 1.3). The chemical modification introduced to obtain HYADD does not affect the relevant features of the biopolymer, such as charge density along the chain and the swelling ability in addition to its interaction behavior with metabolites and cellular material in the synovial matrix. The slight modification, however, induces a strong change in the properties of the system: while native HYA starts to form viscous solutions around volume fractions of $5 \cdot 10^{-2}$ g/ml, HYADD solutions become stable hydrogels above a polymer concentration of only $3 \cdot 10^{-3}$ g/ml.

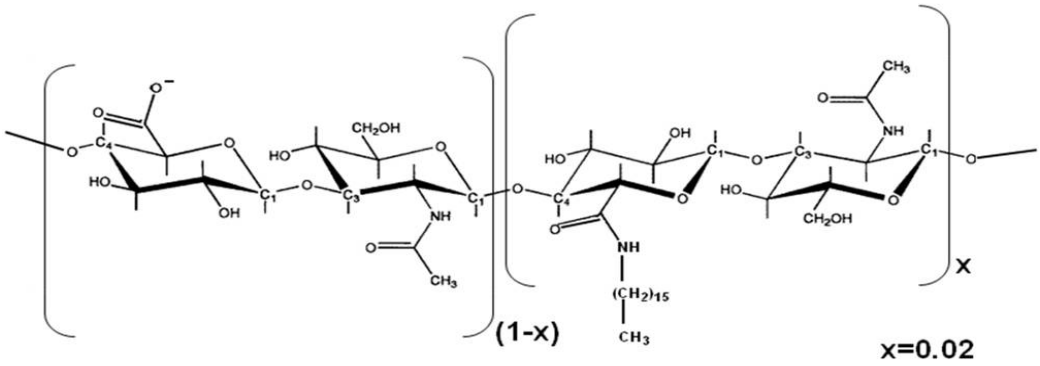

Figure 1.3: Molecular structure of the chemically modified form of hyaluronan chain, HYADD, hereafter investigated

HYADD has recently been tested in an ovine meniscectomy model of osteoarthritis: its effect appeared in a reduction of vascularity and intimal hyperplasia and in an increase in the synthesis of high molecular weight HYA by synovial fibroblasts[1]. From these first tests and the beneficial consequences, HYADD is expected to have a positive clinical effect in joint

mobility and function.

To investigate the structure of HYA and HYADD gels, small angle experiments were carried out using both neutrons and X-rays. A comparative analysis of the information obtained by the two probes, allowed to derive the characteristic lengths describing the organization of the chains in the natural and in the chemically modified preparations.

Aiming to study also the dynamics of the different gels components, we performed several incoherent neutron scattering experiments. As it will be explained in detail in the following chapter, a big advantage of neutrons among other probes such as X-rays, is the possibility to enhance the signal of a specific component of the system probed using isotopic labeling. For the considered gels we prepared samples both in D_2O and in H_2O in order to have information on the dynamics of the polymer chains and of the solvent respectively.

Besides the main research on hydrogels, during my PhD some interesting side-projects were developed thanks to collaborations with other research groups . The first collaboration was with the group of Prof. Santi at the Pharmaceutical Department of Parma University, focused on the investigation of an innovative system used as a drug delivery platform, denominated Patch-non-Patch® [2,3].The technology of Patch-non-Patch® substitutes the multistructure typical of standard transdermal patches: backing layer, drug reservoir and adhesive are condensed in a single layer and the resulting film is very thin, flexible and mechanically resistant and it can be therefore adapted to skin irregularities and joints. An important feature for applications of Patch-non-Patch® is its electrical conductivity, absent in any other form of patch: an electrode, for instance, could be placed directly onto the patch to allow iontophoresis to increase the permeation of the active molecule inserted. The biocompatibility of such a system is guaranteed by its high permeability to water, that avoids all

problems of skin irritation encountered with the use of impermeable patches. The small amount of the adhesive present in the formulation, gives the patch the peculiar characteristic of being not self adhesive in the dry state: the adhesiveness is restored when it is applied to the skin in presence of a small amount of water. In terms of adhesion, the amount of water used for film application can be critical below a limiting value (4.5 μl/cm^2 corresponding to 20 % wt water/wt patch)[4]. Absorbing water, the film swells and the drug release can take place. Film hydration is a key feature for the functioning of the system and it is very important to understand the role and behavior of water to optimize the power of the application. The functioning of the system has been already tested for several small molecules such as caffeine, lidocaine, sumatriptan, etc...[2,5,6].

Focusing on the drug release kinetics, all the drug molecules inserted in the Patch-non-Patch® show a similar behavior: the delivery of the active species is switched on by the hydration of the polymeric film and it is characterized by a very short time lag. In the case presented in this thesis, lidocaine is the active molecule chosen, due to its favorable characteristics (low molecular weight, high water solubility, easy analytical method). This molecule is a chemical commonly used for anti-arrhythmic or local anesthetics: in the latter case, for example lidocaine acts stabilizing the neuronal membrane by inhibiting the ionic fluxes required for the initiation and conduction of impulses, thereby effecting local anesthetic action. Local anesthetics of the amide type are thought to act within sodium channels of the nerve membrane. Diffusivity of lidocaine through the polymer film has been investigated by macroscopic permeation experiments[5]: it has been shown that the permeation profiles are not linear with time, but they typically show a fast initial permeation, followed by a reduced flux. The permeation data become linear when plotted versus the square root of time suggesting a matrix-type control of drug delivery by the film ac-

cording to its hydration level[6].

In order to probe the diffusivity, at a molecular level, of water and of drug molecules through the film we performed a quasi-elastic neutron scattering (QENS) experiment using the time-of-flight spectrometer IN5 at the Institut Laue Langevin (ILL) in Grenoble, France. In this context QENS is one of the few techniques, with pulsed field NMR, allowing to study the patch 'alone', i.e. without the need of any additional support such as a porous membrane that could affect the diffusivity measurements.

Another important collaboration carried on during the PhD was with the group of Italian and French researchers in charge of the maintenance and development of the back-scattering spectrometer IN13 at ILL. Thanks to a financial support from the Italian National Center of Research (CNR) I had the chance to spend one year and a half at ILL, where I joined the IN13 group and I took part to the technical and scientific group activities. In Chapter 3 the functioning and specific characteristics of IN13 will be described; finally some examples of the instrumental improvements and scientific experiments to which I took part, will be presented.

Chapter 2

Radiations to probe soft matter

Dealing with soft matter many forms of radiations such as X-rays, neutrons, electrons, etc. can be used to investigate different aspects of the materials studied. This chapter wants to give a general overview of the most exploited scattering techniques, with particular attention on neutrons and X-rays, employed to study the structure and the dynamics of the polymeric systems described in the following chapters.

2.1 How to probe dynamical processes

Figure 2.1 shows the comparison between the time ranges and the spatial resolutions of different experimental methods useful to probe dynamical processes in polymeric systems.

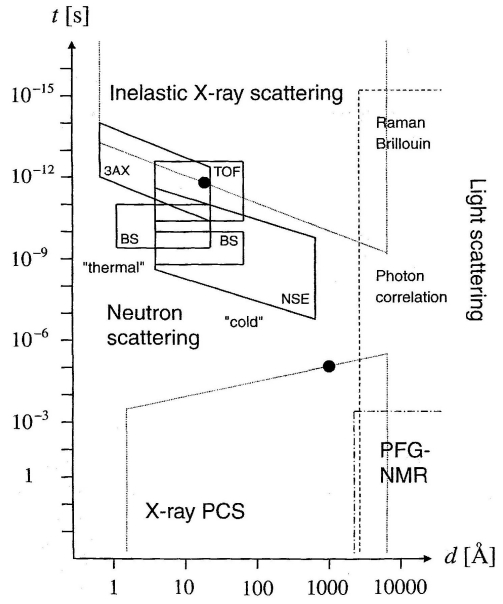

Figure 2.1: Space and time ranges accessible by the different scattering techniques.

In this thesis, neutrons are the probe chosen to study gel dynamics through experiments on time-of-flight and backscattering spectrometers. For macromolecular systems in general, it is of particular interest the time region from pico- to nanoseconds, in which several processes take place: if the focus of the analysis is, for instance, on a single polymer chain, one can study from local dynamics of molecular bonds, typically of the order of picoseconds, to slower reptation processes; on the other hand, when investigating a polymer gel on the whole, motions that can be revealed are closely connected to intermolecular interactions and those between the solvent and the polymer chains. Depending on the energy transfer between neutrons and macromolecular system, it is possible to study vibrational, rotational and translational motions that take place inside the sample. The energetic gap between two adjacent vibrational levels is big compared to neutron energy and the transition from one level to the other

produces a clear and discrete peak in the inelastic spectrum. Rotations and translations instead need lower quantity of energy: therefore it is possible to neglect the quantum effects and to consider the system studied with a classical approach. Rotational and translational motions produce an enlargement of the elastic line at $\omega = 0$: the technique that studies these phenomena is called Quasi Elastic Neutron Scattering, *QENS*.[7] To understand which kind of information such a technique can give, in the following a brief recapitulation of the basics of inelastic neutron scattering is presented.

The fundamental quantity measured in a neutron scattering experiment is the *double differential cross-section*:

$$\frac{\partial^2\sigma}{\partial\Omega\partial\omega} = N\frac{k_f}{k_i}\left((\langle b^2\rangle - \langle b\rangle^2)S_{inc}(Q,\omega) + \langle b\rangle^2 S_{coh}(Q,\omega)\right) \tag{2.1}$$

The multiplication of this quantity by the flux of incoming neutrons gives the number of neutrons scattered into a solid angle element $d\Omega$ with an energy transfer $\hbar\omega$. In Equation 2.1, N is the number of scattering elements in the sample, k_f and k_i are the final and incident wave vector respectively, b is the scattering length characteristics to each nucleus and to the relative spin orientation of the nucleus and the incident neutron. The scattering functions $S_{coh}(Q,\omega)$ and $S_{inc}(Q,\omega)$, provide a direct link to the microscopic motions of the atoms.

$$S_{coh}(Q,\omega) = \frac{1}{2\pi}\int d^3r \int dt e^{i(Q\cdot\mathbf{r}-\omega t)}G(\mathbf{r},t) \tag{2.2}$$

The previous equation shows that the *coherent* scattering function, S_{coh} (Q,ω), is the double Fourier transform in space and time of the density-density correlation function[8]

$$G(\mathbf{r},t) = \frac{1}{\rho_0}\langle\rho(\mathbf{0},0)\rho(\mathbf{r},t)\rangle \tag{2.3}$$

that can be classically expressed in terms of the atom position

$$G(\mathbf{r},t) = \frac{1}{N}\Big\langle \int d^3\mathbf{r'} \sum_{i,j} \delta(\mathbf{r} - \mathbf{r'} + \mathbf{r}_j(t))\delta(\mathbf{r'} - \mathbf{r}_i(0))\Big\rangle \tag{2.4}$$

In the classical picture $G(\mathbf{r},t)$ can be interpreted as the probability density of finding, at time t, an atom at a distance **r** from the position of another atom at time 0.

With an analogous approach one derives that the *incoherent* scattering function, $S_{inc}(Q,\omega)$ in Equation 2.1, is the double Fourier transform in space and time of the classical self correlation function[8]

$$G_{self}(\mathbf{r},t) = \frac{1}{N}\Big\langle \int d^3\mathbf{r'} \sum_{i} \delta(\mathbf{r} - \mathbf{r'} + \mathbf{r}_i(t))\delta(\mathbf{r'} - \mathbf{r}_i(0))\Big\rangle \tag{2.5}$$

The above function is the probability density of finding an atom at time t at a distance **r** from its position at time 0.

When performing experiments on organic or biological materials, the inelastic neutron scattering signal is dominated by the high incoherent contribution of hydrogen: the reason is that its incoherent scattering length and consequently its incoherent cross section (see Table 2.1) is about ten times higher than that of other atoms also common in soft matter (C, N, O,...).

Table 2.1: Neutron scattering cross sections of common elements in soft matter (1 barn = 10^{-24}cm^2).

Element	$\sigma_{coh} = 4\pi\langle b\rangle^2$ (barn)	$\sigma_{inc} = 4\pi(\langle b^2\rangle - \langle b\rangle^2)$ (barn)
C	5.551	0.001
H	1.7568	**80.26**
D	5.592	2.05
O	4.232	0.0008
N	11.01	0.5
S	1.0186	0.007

Since hydrogen atoms are abundant and uniformly distributed in organic and biological macromolecules, the organization and behavior of the latter is reflected by the signal scattered by protons. The scattering from hydrogen is mostly incoherent, providing therefore information on single particle dynamics.

Assuming the hypothesis that all the atoms interacting with neutrons are identical and dynamically equivalent, the incoherent scattering function can be expressed as the convolution of the contribution to the scattering of the different kinds of motions[7]:

$$S_{inc}(Q,\omega) = S^T_{inc}(Q,\omega) \otimes S^R_{inc}(Q,\omega) \otimes S^V_{inc}(Q,\omega) \tag{2.6}$$

The three components in Equation 2.6 are due respectively to translational, rotational and vibrational motions. Equation 2.6 is appropriate for systems such as liquids in which long-range translational motion can take place; in bulk sample the translational scattering function is substituted by a term related to lattice phonons. Referring to calculations that can be found for

instance in reference[7], we report here only the result of the above convolution when considering only the quasi-elastic region of a spectrum, that is the case of the experiments hereafter described:

$$S_{inc}(Q,\omega) = exp(-\langle u^2\rangle Q^2/3)\left[S^T_{inc}(Q,\omega) \otimes S^R_{inc}(Q,\omega)\right] \tag{2.7}$$

The exponential factor in Equation 2.7 represents the effect of internal molecular vibrations: its exponent is the so called Debye-Waller factor in which $\langle u^2\rangle$ denotes the mean square displacement of the atom from its equilibrium position. $S^T_{inc}(Q,\omega)$ and $S^R_{inc}(Q,\omega)$ are two basic quantities in any QENS experiment.

The most general expression of an incoherent neutron scattering function, representing indistinctly a translational or rotational motion, is through the sum of a purely elastic and a quasi-elastic term:

$$S^i_{inc}(Q,\omega) = A_0(Q)\delta(\omega) + S^{qel}_{inc}(Q,\omega) \tag{2.8}$$

The width of the quasi-elastic component $S^{qel}_{inc}(Q,\omega)$ provides information on the characteristic times of the motions represented. The coefficient of the delta function, $A_0(Q)$, is called *Elastic Incoherent Structure Factor* (EISF): it is the space Fourier transform of the final distribution of the scattering nuclei and its value can be only between 0 and 1. In general, if the separation between the purely elastic component and the quasi-elastic one can be performed, the EISF is a measurable quantity, evaluated from the ratio of the integrated intensities, $I_{el}(Q)$ and $I_{qel}(Q)$, corresponding to the elastic and quasi-elastic part of a spectrum respectively.

$$A_0(Q) = \frac{I_{el}(Q)}{I_{el}(Q) + I_{qel}(Q)} \tag{2.9}$$

In the analysis of the elastic component of a QENS spectrum, different expressions of the EISF can be used depending on the kind of geometry assumed for the atoms seen as immobile (i.e. giving an elastic signal) in the

particular system investigated. In the following chapters all the models adopted will be described in details.

2.2 Structural investigation

Polymeric materials exhibit a diverse range of structures ranging from linear chains to block copolymers to dendritic or hyperbranched architectures in which inter- and intramolecular interactions are determined by the chemical composition of each architectural subunit. As a result, polymeric systems show organization phenomena over various length scales. A comprehensive structural analysis requires experimental methods covering length scales from interatomic distances up to macroscopic dimensions. Being interested on length scales from Å to μm, various scattering techniques need to be combined to detect and characterize structures at various size scales:

- Wide angle X-ray diffraction experiments are sensitive to interatomic spatial correlations in the Å to nanometer range.
- Small angle X-ray scattering is used to investigate structures in the size range between 1 and 60 nm characteristic for semicrystalline polymers, copolymers and nanocomposites.
- Neutron scattering experiments represent a complement to X-rays thanks to the unique possibilities, offered by neutrons, of controlling scattering length contrast by isotopic labelling (deuteration is the most common).
- Wide and small angle light scattering extend the possibility of structural analysis up to the micrometer range.

Table 2.2 shows a summary of the above mentioned techniques and of the kind of inhomogeneities they are sensitive to.

Table 2.2: Comparison between radiations used in scattering.

Type of radiation	**X-rays**	**Neutrons**	**Electron**	**Laser light**
Wavelength range	$0.1 - 5$ Å	$1 - 15$ Å	0.1 Å	1 μm
Sensitive to inhomogeneities	Electron density	Density of nuclei	Electron cloud	Polarizability
Scattering methods	Small and Wide angle X-ray scattering (SAXS/WAXS)	Small Angle Neutron Scattering (SANS)	Low Energy Electron Diffraction (LEED)	Static Light Scattering (SLS)

Neutron scattering is the technique of choice for condensed matter investigations in general because thermal/cold neutrons do not deposit energy in the scattering specimen. To give some numbers, neutrons of 1 Å wavelength have much lower kinetic energy (82 meV) than X-rays and electrons of the same wavelength (12 keV and 150 eV respectively).

In comparison to other structure determination methods, such as NMR or X-ray crystallography, small angle scattering (SAS) allows to overcome some restraints. For example, NMR is limited to protein size, whereas SAS can be used for small molecules as well as for large multimolecular assemblies. Structure determination by X-ray crystallography may take several weeks or even years, whereas SAS measurements take days. However, with SAS it is not possible to measure the positions of the atoms within the molecule. In the following a brief description of the basics of SAS theory is presented.

For structural studies of soft matter systems, only the elastic coherent scattering processes, i.e. those with zero energy transfer, are of interest. Referring to the expression of the double differential cross section in Equation 2.1, one has to consider only the *differential cross section* $d\sigma/d\Omega$: this quantity represents the probability of a particle of the incident beam to be scattered out of the sample into the solid angle $\delta\Omega$ and it contains all the information on the structure of the sample.

If we look at a polymer chain as an assembly of N atoms at individual position $\mathbf{r}_i$ and fixed orientation, the scattering of a generic radiation leads to interference phenomena: the incident plane wave interacts with the atoms hit and the spherically symmetric waves scattered from each atom i at position $\mathbf{r}_i$ with wave function A_i, interfere. The differences between the techniques are related to the nature of the fraction of radiation scattered by atom i, i.e. the already mentioned scattering length b_i. Using the Born approximation[9], the total scattering can be written as the sum of N wave functions A_i:

$$A(\boldsymbol{Q}) \propto \sum_N b_i exp[-i\boldsymbol{Q}\boldsymbol{r}_i] \tag{2.10}$$

Since in SAS the observed length scale is much larger than interatomic distances, the sum can be replaced by an integral

$$A(\boldsymbol{Q}) \propto \int_V \rho(\boldsymbol{r}_i) exp[-i\boldsymbol{Q}\boldsymbol{r}_i] dr \tag{2.11}$$

$\rho(\boldsymbol{r}_i) = \sum b_i/V$ is the scattering density distribution and for different radiations it is proportional to different quantities (see Table2.2).

If we consider n polymer chains each composed of N atoms in a solvent, the total scattering $F(\mathbf{Q})$ is the sum of the scattering of each chain:

$$F(\boldsymbol{Q}) \propto \sum_k A_k(\boldsymbol{Q}) exp[-i\boldsymbol{Q}\boldsymbol{r}_k] \tag{2.12}$$

For an isotropic distribution of the scattering elements, the differential scattering cross section as a function of momentum transfer Q is obtained averaging over all the orientations and multiplying Equation 2.12 by its complex conjugate

$$\frac{d\sigma}{d\Omega}(Q) \propto \left\langle F(\boldsymbol{Q})F*(\boldsymbol{Q})\right\rangle = \langle \sum\sum b_i b_j exp[-i\boldsymbol{Q}(\boldsymbol{r}_i - \boldsymbol{r}_j)]\Big\rangle \tag{2.13}$$

This fundamental equation is the base to calculate model scattering laws for SAS. It can be rearranged to

$$\frac{d\sigma}{d\Omega}(Q) \propto (\rho - \langle\rho\rangle)^2 \int_V P(r) exp[-iQr]dr \tag{2.14}$$

The integral term is a sum of the so-called *form factor*, that contains information on the conformation of the individual polymer chain, and of the *structure factor*, that gives information on the interaction of the n polymer chains in solution. ρ in Equation 2.14 is the scattering density of the polymer and $\langle\rho\rangle$ is the average scattering density of the solution. Their difference is the *contrast* between the scatterer (polymer chain) and the reference medium (the solvent) and it is a radiation specific. In the case of neutron scattering b varies without any regularity along the periodic table and isotopes of a given nucleus can have values of b dramatically different (See cross sections values in Table 2.1); moreover, for neutrons, b depends on the direction of the nuclear spin. Isotopic labeling is therefore a very common technique to change the scattering contrast in the investigated system in order to highlight the effect of a specific component.

On the other hand, for X-rays the scattering length b is proportional to the number of electrons Z in an atom, through the electron radius r_{el}:

$$b_{el} = r_{el} Z \tag{2.15}$$

For X-rays it is not straightforward to change the contrast since it requires, for example, the use of heavy metal salts or sugars as additives

which can strongly affect the properties of the system. An interesting option for soft matters analysis is to consider X-rays with energy close to the absorption edge of an atom (*anomalous scattering*).

2.3 Performing a real experiment

All the theory stated above refers to the interpretation of the *theoretical* scattering functions. When performing a *real* experiment however, the measured scattering intensity depends not only on the behavior of the atoms in the sample, but also on instrumental resolution. The latter can be a function either of the energy or of the wave vector.

$$S_{measured}(Q,\omega) = S_{theoretical}(Q,\omega) \otimes S_{resolution}(Q,\omega) \tag{2.16}$$

To measure the instrument resolution one normally performs a run on a specific reference: for incoherent neutron scattering experiments the reference taken is normally Vanadium, a purely incoherent scatterer that gives only an elastic peak at room temperature. Since incoherent scattering is by definition isotropic, a Vanadium run is useful also to consider other instrumental parameters in the data reduction such as the different efficiency of each detector and the different transmission of each analyzers. In a SAS experiment these instrumental characteristics are taken into account measuring references such as water or plexiglass that give Q-independent intensities. In general, also the Q-resolution of the small angle diffractometers has to be considered: in the SAXS experiment hereafter presented, the instrumental resolution is so high (see Chapter 4) that we approximated it to a delta function; the resolution of a neutron diffractometer is lower than that of an X-ray one, however the samples investigated in this thesis do not show a well defined periodic structure and we are confident not to loose structural information neglecting the resolution.

Chapter 3

The backscattering spectrometer IN13

3.1 Functioning of a backscattering spectrometer

Figure 3.1 represents a general scheme of a spectrometer for inelastic scattering.

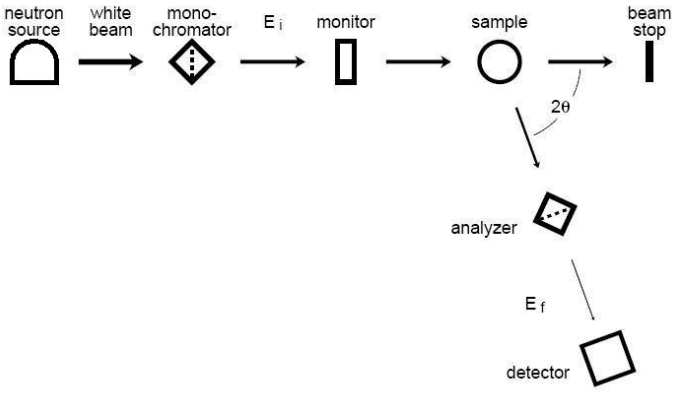

Figure 3.1: Layout of a typical inelastic spectrometer.

Incident neutrons are selected in energy by a *monochromator*, also called *primary spectrometer*: only neutrons having a certain energy E_i can continue their run. Those which reach the sample passe throught a *monitor*, a neutron counter with high transmission, and then they enter in the so called *secondary spectrometer*: there, the scattered neutrons are registered as a function of the scattering angle 2θ and the energy E_f. Depending on the kind of instrument, the energy selection can occur in two different ways: in Time-of-Flight (TOF) spectrometers, neutrons energies are selected and measured via their velocity v and, to do this, *choppers* are used as monochromator; on the other hand, in crystal spectrometers, incident neutrons energies are selected using Bragg reflection from crystals according to neutrons incident wavelength, λ:

$$n\lambda = 2d_{hkl}sin\theta \tag{3.1}$$

d_{hkl} is the interplanar distance of lattice planes with Miller indices *h*,*k*,*l* and θ is the angle of reflection from these planes.

In an ideal spectrometer, a well defined wave vector k_i (remember the inverse relation $k = 2\pi/\lambda$) is selected by an ideal monochromator and after the interaction with the sample, it is transformed into an equally well defined k_f. Experimentalists would not look for such an instrument, since the resolutions would be perfect, but the count rates would be equal to zero. In a real crystal spectrometer the resolution is limited by several factors such as the absorption in the monochromator crystal, imperfections of the crystal as mosaicity (non-parallelity) of the Bragg planes and divergences of the incoming and outcoming beams. The combination of all these factors leads to:

$$\frac{\Delta\lambda}{\lambda} = \frac{\Delta d}{d} + \cot\Theta\delta\Theta \tag{3.2}$$

where d is the lattice spacing and $\delta\Theta$ indicates the angular aperture

of the beam. Normally the ratio $\frac{\Delta d}{d}$ can be neglected in comparison to the other term and the resolution depends only from $\delta\Theta$. In backscattering (BS) geometry however, $2\Theta \sim 180°$ and $\cot\Theta$ in Equation 3.2 goes to zero: in this case the wavelength spread of the Bragg reflected beam depends mainly on $\frac{\Delta d}{d}$. In a backscattering spectrometer, both monochromator and analyzers operate under backscattering conditions: commonly, relative energy resolutions between 10^{-3} and 10^{-4} can be obtained. For obvious reasons, in such an instrument, the sample cannot be placed in the incident beam path and a deflector is needed to deviate the beam backscattered by the monochromator into the secondary spectrometer. Once in there, neutrons backscattered again from the analyzers have to transverse the sample a second time before reaching the detectors. The latter receive however also neutrons scattered directly from the sample without being energy analyzed: to avoid the count of these uninformative particles, every backscattering instrument needs a chopper to pulse the beam going to the sample. The "good" neutrons are then distinguished from the others by their different time of flight.

With all these general information we can now examine the details of IN13: IN13 is a thermal ($\lambda = 2.23$ Å) neutron backscattering spectrometer with high energy resolution and high momentum transfer. Classical applications of IN13 span from material science to solid state physics to chemistry, but recently the instrument has been exploited at most to study biological compounds such as model membranes or proteins in order to investigate the relations between the dynamics of such systems and their functionality.

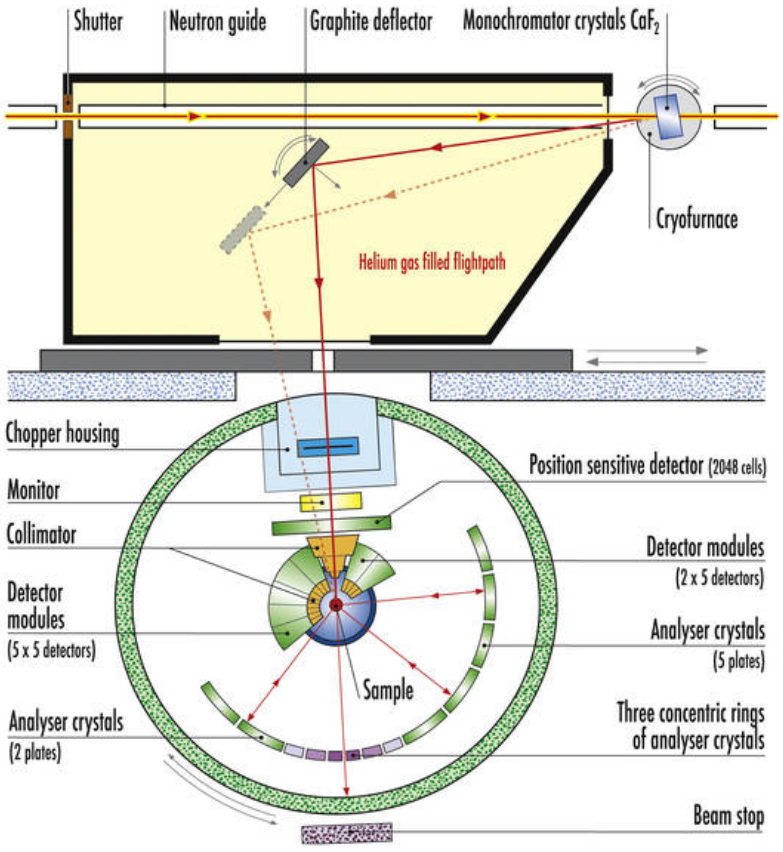

Figure 3.2: Scheme of IN13.

On IN13 the monochromator is a CaF_2 (422) crystal oriented in near-BS geometry that allows to achieve a resolution (FWHM) up to 8μeV. For inelastic experiments, the energy of the incident beam onto the sample is scanned normally varying the temperature of the monochromator crystal at a fixed Bragg angle. A pyrolytic graphite deflector with variable curvature is used to deviate and focus the beam onto the sample measured. Once scattered, the neutrons are energy analyzed by a set of seven spherically curved crystal analyzers (again CaF_2 (422)) and by a central position sensitive detector (PSD) made by three circular analyzers (He^3 detector

tubes) to cover the small angles region.

3.2 Being part of IN13 team

Being part of the team responsible of an instrument in a large scale facility like ILL means to furnish a functioning and efficient instrument to users that come for few days and want to perform fruitful experiments. To make it possible, when the reactor is operating, it is important to assist the experimentalists during their experiments and, during the reactor shutdown periods, the team has to work continuously to make all the needed technical improvements following the standards requested by the hosting institution. While I was at ILL, IN13 group was made by the two instrument responsibles, Dr. Francesca Natali and Dr. Judith Peters, a technician and another PhD student, Marcus Trapp. Within ILL, IN13 belongs to the framework of 'Collaborating Research Groups' (CRG), which can build and manage instruments on ILL beamlines to carry out their own research programmes.

During my stay, I was involved in all scientific and technical activities of the group. An example of scientific project to which I took part is the test of the high pressure system developed at the ILL within the IN13-CRG. Such an apparatus has been test to work up to 7 kbar, namely the highest pressure reachable: the functioning mechanism is characterized by a primary pressure hand pump (max P=700 bar) and a pressure intensifier (max P=7 kbar), connected one to the other through a system of pressure gauges of accuracy ± 10 bar, stainless steel fittings and valves.

Figure 3.3: High pressure cylindrical cell made from an inox capillary tube ($d_{int} = 0.5$ mm, $d_{ext} = 1.6$ mm) enrolled into an annular geometry (height=50 mm; diameter=36 mm). The sample volume that can be illuminated by the beam is 1.3 cm^3.

Pressure is an effective modulator of biochemical processes as, for instance, it inhibits bacterial growth, affects virus vitality and activates/ inactivates enzymatic reactions. The chance to perform experiments in high pressure conditions it is therefore very important either for basic biophysical and biochemical studies or in applied research related, for example, to food technology[10] and to medical and pharmaceutical applications.[11] In particular, the relationship between structure/dynamics of proteins and their function can be revealed in detail considering the pressure parameter. For instance, increasing pressure, modifications of fundamental physical features of the protein-solvent system can occur; moreover monomeric proteins denaturate above 3 kbar while multimeric pro-

teins can dissociate at lower pressures, i.e. between 1 and 3 kbar.

Under the supervision of Dr. Daniela Russo, responsible for IN13 high pressure cell, several experiments were performed to test the high pressure environment for different systems. In particular the last elastic neutron scattering experiment carried out when I was at ILL aimed to investigate the dynamical changes induced by high pressure on lysozyme and $\beta-$lactoglobulin, two small monomeric globular proteins. Lysozyme, known to be immediately inactivated by pressure[12], was studied at 298 K in two buffers (tris and acetate) undergoing pressure cycles from 1 bar up to 5.5 Kbar. For $\beta-$lactoglobulin we investigated the reversible denaturation process taking place between 1 and 1000 bar and at temperature always fixed at 298 K. The aim was to compare the mean square fluctuations of the two proteins in order to understand the different steps in the denaturing processes. Elastic neutron scattering proved to be a useful microscopic technique for the investigation of changes in protein flexibility and resilience induced by high pressure. The analysis of the data collected from this experiment and the results obtained have been already published.[13]

Furthermore I was involved in a project, developed within a collaboration between Dr. Natali and the group of Milan University leaded by Prof. Laura Cantù, focusing on the characterization of model phospholipid membranes enriched with sugar moieties. It is known that the latter are present in many macromolecules of biological relevance, but their importance for living matter has still to be understood. In the project here introduced gangliosides are the sugar-containing molecule considered. Gangliosides are double-tailed amphiphilic molecules with a complex polar headgroup formed by several sugar units and two apolar tails. They are naturally abundant in neuronal plasma membranes, where they are known to participate to cell recognition and transmembrane signal trans-

duction.[14] While I was working with Dr. Natali, I took care in particular of the analysis of preliminary QENS data to test two systems: one was composed of a stack of dry oriented bilayers of dimyristoylphosphatidylcholine, DMPC, while the other consisted in an analogous stack of model membranes in which GM1[15], a ganglioside with five sugar rings in the headgroup, had been inserted. The scientific interest is double: on one side there is the characterization of the dynamics of simple model membranes, that since many years remains a hot topic for many researchers and, nevertheless, there are still a lot of question marks about it; on the other side it is important to understand the eventual influence of the ganglioside on pure membrane dynamics. A whole PhD thesis could be written about membranes dynamics but this is not the case: the above paragraph wants just to be an example of the themes I approached while being an IN13 PhD student. The possibility to work in such a stimulating environment, and the chance to interact with different scientists has been a great opportunity to learn and enrich my knowledge about the main scientific topics in modern physics/biophysics.

Besides the scientific aspect of my stay at ILL, I took also part to the technical development of IN13. In particular I want here to describe as example the improvements concerning the optimization of the beam alignment. The optimization process started after having discovered a bad functioning in the deflector alignment. The deflector is made by several blocks of pyrolytic graphite, placed on a track in order to be able to move during an inelastic experiment to collect the beam at every energy and deflect it onto the sample.

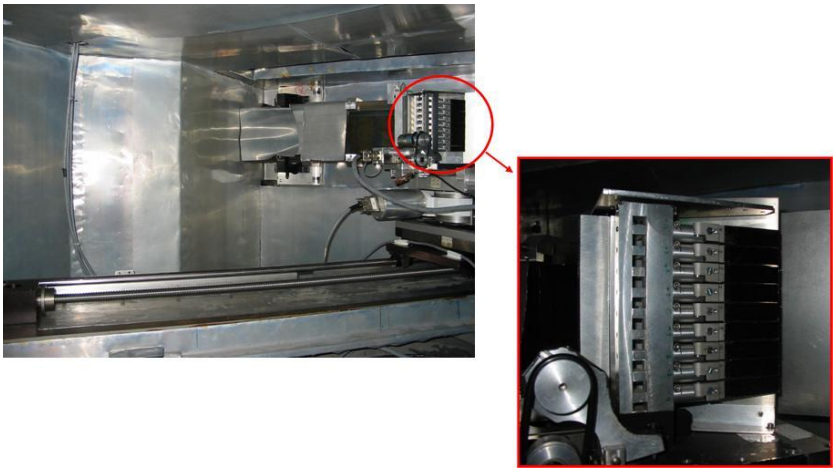

Figure 3.4: Pictures of the deflector chamber. The picture on the right is a zoom on the pyrolytic deflector.

The motions of the deflector are performed through motors, placed in the deflector chamber, that permit the displacements in all the directions; these motors are controlled by encoders, i.e. electronic devices needed to put in communication the computers where the positions of the motors are set and the motors themselves that have physically to perform the displacements. The source of the problem in the deflector system was recognized to come from the encoders that did not work properly and were therefore changed. Making this substitution it became evident the need of a way to be able to remotely control the position of the deflector without the need to open the casematte. We decided therefore to insert a laser and an infrared camera in the deflector chamber.

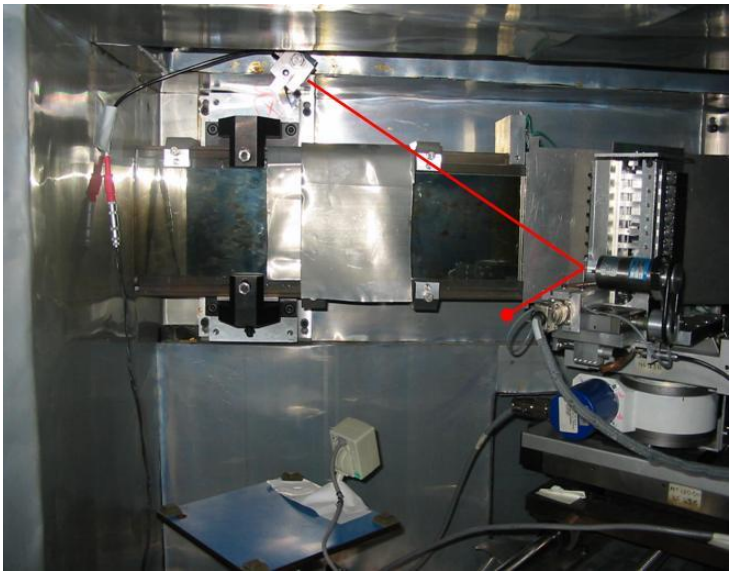

Figure 3.5: Picture of the deflector chamber in which the laser has been inserted. The red line has been drawn to give an idea of the functioning of the system.

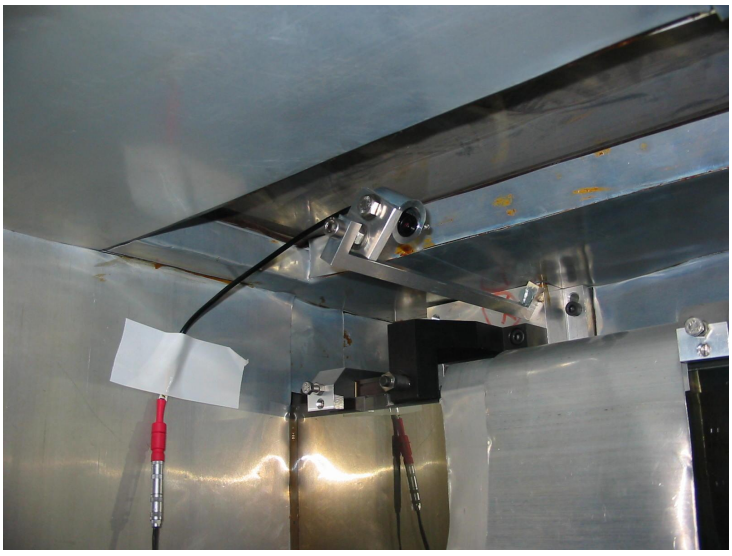

Figure 3.6: Detail of the laser inserted.

Outside the carousel a switch was placed to turn the laser on and off. When it is on, the laser beam points on a small mirror glued on the back of the deflector and it is then reflected on the Cadmium wall below the neutron guide. On this wall we marked the expected point of the reflection for the best position of the deflector in an elastic experiment. The infrared camera was connected to a monitor placed in the control cabin: from this monitor it is now possible to control online, i.e. when the neutron beam is on and an experiment is going, the position of the reflected laser beam and therefore of the deflector.

The last step in the process of optimization of the beam alignment concerned the control of the position of the sample in the beam. The old methods used on IN13 consisted in taking a picture of the sample, hit by neutrons, with a polaroid camera that had to remain exposed for almost 5 minutes. Such a system was updated to ILL standards substituting the polaroid with a CCD scintillator camera.

Figure 3.7: CCD scintillator camera adopted to reveal the sample position in the beam

With this new system now it is possible to visualize the sample in the beam in real time from outside the experimental zone. Figure 3.8 shows to pictures taken during a test of the camera performed using a cadmium pointer as sample. Panel a) shows the results of an exposure time of 10 seconds and its quality is comparable to that of the images obtained from the Polaroid camera after 5 minutes.

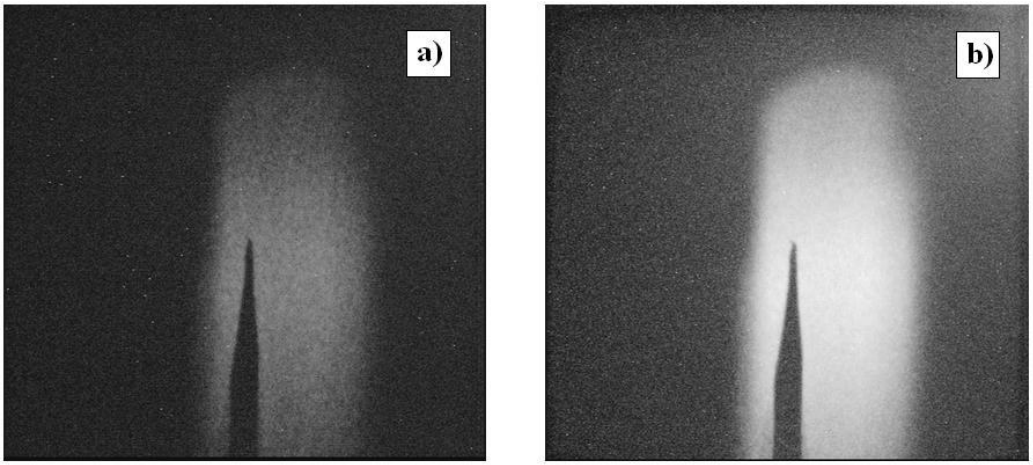

Figure 3.8: Images of a cadmium pointer placed as a sample in the neutron beam taken with the new installed camera: a) Picture after 10 seconds b) Picture after 20 seconds

.

Chapter 4

Hyaluronic acid gels

Since Karl Meyer isolated hyaluronic acid (HYA) for the first time in 1934, this polysaccharide became one of nature's most versatile and fascinating macromolecules. Many scientific studies ensued on it,[16,17] however several aspects of HYA remain to be understood. HYA is of particular interest in the field of bio-medical applications, for instance in treatments to heal joints and cartilage.

Due to the ease with which its chemical composition can be modified, different functional groups can be introduced in HYA structure. In the following, we will describe the study performed on a particular derivatized form of HYA, called HYADD: as mentioned in the introduction, HYADD is obtained grafting hexadecylic chains on HYA backbone, with a degree of modification between 1 and 3% of the repeating units. This small chemical modification produces dramatic macroscopic effects, in particular it gives the system the possibility to become a gel at concentrations 10 times lower than those needed for natural HYA. Such a peculiarity broadens significantly the possible applications of HYADD respect to pure hyaluronate.

Hereafter we will present neutron and X-ray experiments carried out to investigate structure and dynamics of HYADD gels in relation to their

natural counterpart, HYA gels, taken as reference. This research represents a part of a wider project directed toward a more complete characterization of HYADD gels; the project involves several research groups experienced in different experimental techniques. In this framework it has been very important the work performed by Dr. Ivana Finelli, working within the group leaded by Prof. G. Paradossi, at University of Rome Tor Vergata. It is worth mentioning in particular the detailed study on HYADD viscoelastic properties realized through rheology experiments. The latter showed that, while HYA forms purely viscous solutions, in HYADD systems the elastic behavior prevails onto the viscous one: this information tells that the reversible links that form between HYADD chains are rather stable and resistant and the resulting system is a stable gel. Moreover it has been proved that, if we first introduce an external stress to make the gel flow and we then remove the stress source, HYADD recovers all its elastic characteristics. In a treatment, for instance, to heal a cartilage, the gel has first to flow through a syringe and then it needs to be able to rearrange its original structure in order to be a valid substitute to the degraded cartilage: the viscoelastic properties of HYADD make it a good candidate for such kind of applications.

Concerning the investigation on structure and dynamics of HYADD gels presented in this chapter, we will first give a short description of the standard procedure followed to prepare the samples; we will then present the analysis of gel structure as a function of concentration, investigated with SAXS and SANS. Consequently the study on polymer dynamics in the gels will be described throughout the analysis of the elastic neutron scattering data taken using IN13 at ILL and the analysis of the quasi-elastic data obtained from SPHERES, the high resolution spectrometer at the reactor FRMII in Munich. In the last section of the chapter we will show the results obtained on solvent dynamics probed using NEAT, a time-of-flight

machine at BENSC reactor in Berlin. Figure 4.1 wants to give an overview of the energy- and wave vector-ranges explored with the different instruments exploited to probe both polymer and solvent dynamics. The lower limit in the energy range is given by instrumental resolution. For IN13 a single line has been inserted indicating that we carried out only an elastic experiment.

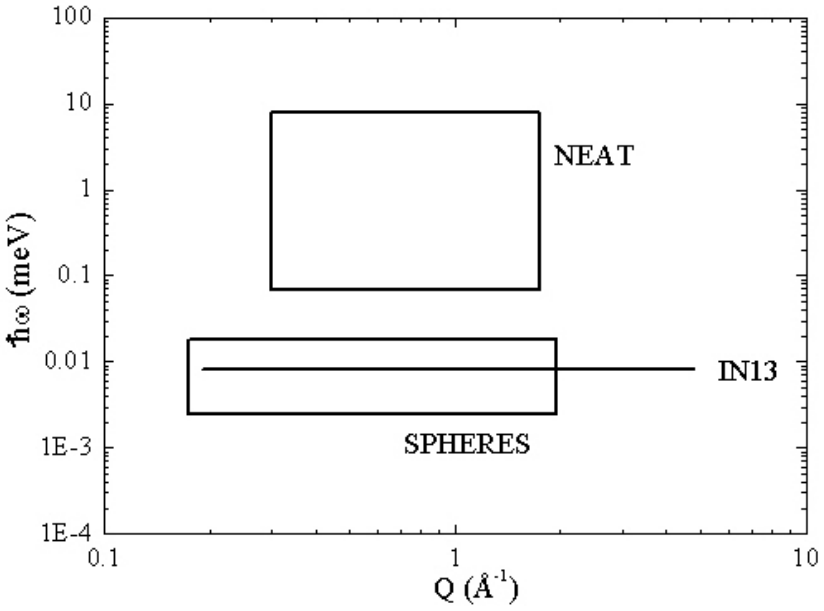

Figure 4.1: Scheme of the energy- and $Q-$ranges explored with the different spectrometers used, namely SPHERES and IN13 for polymer dynamics and NEAT for water dynamics.

4.1 Gel preparation

Hyaluronate tetrabutylammonium salt ($\langle \mathrm{MW} \rangle \sim 700$ KDa), obtained from hyaluronic acid sodium salt produced by a bacterial source , was provided by Fidia Farmaceutici SpA (Abano Terme, Italy) as a freeze-dried pow-

der. Synthesis of HYADD was performed in Fidia Farmaceutici Chemical Research Laboratories. HYA and HYADD hydrogels were prepared by Dr. Ivana Finelli. The standard preparation procedure consists in the dissolution of the polymer in a phosphate-buffered saline (PBS) (pH = 6.9) at concentrations ranging between $3 \cdot 10^{-3}$ and 0.1 g/ml. The positive sodium ions present in PBS neutralize the negative charges characteristic of hyaluronic acid chains and the resulting gel is therefore neutral. After an overnight stirring, the obtained milky dispersion (5 mL) was autoclaved (Carlo Erba, 760 autoclave, Italy) for 15 min in a stoppered glass cylindrical vial: autoclaving was necessary to ensure the production of a sterile material and to obtain a product with good homogeneity.[18] The resulting hydrogel, was finally cooled at room temperature.

For neutron scattering experiments, the gels were prepared in hydrogenated or deuterated buffer to evidence, respectively, solvent and polymer chains behavior (see Chapter 2 for the importance and meaning of the isotopic labeling). It has to be remarked that the ions present in PBS do not significantly alter the scattering length density of pure water and, in the following, we will refer to the buffer as simple H_2O or D_2O depending on the specific case.

4.2 Structure of the polymer chains

4.2.1 Small angle diffractometers

The structure of diluted gels, i.e. of concentration up to $8 \cdot 10^{-3}$ g/ml, was studied with SAXS: the experiment was performed using the high brilliance beamline ID02 at the European Synchrotron Radiation Facility (ESRF) in Grenoble.

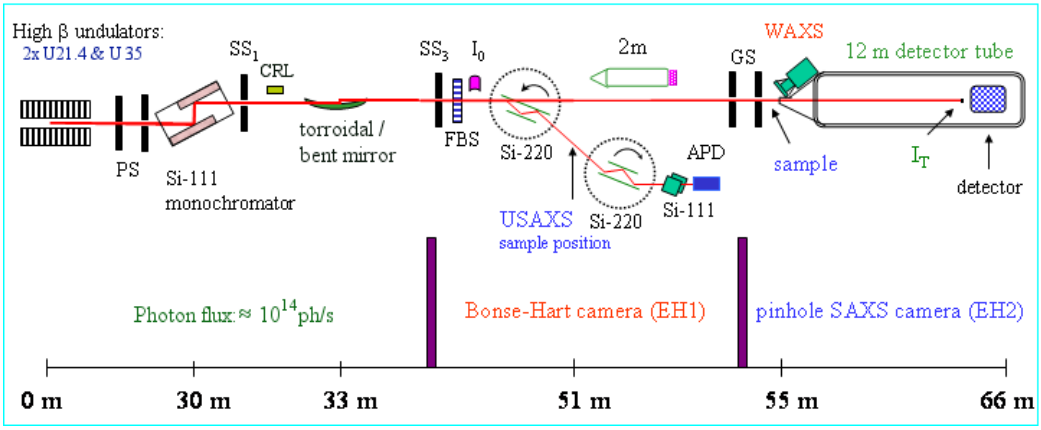

Figure 4.2: Layout of ID02 beamline (image taken from ESRF website).

The incoming beam has dimension of $1\text{mm}\times1\text{mm}$ and a wavelength λ of 0.1 nm (12.4 keV), giving a resolution $\Delta E/E = 2\times10^{-4}$. Positioning the detector at 1 and 5 m from the sample, the explored Q-range covers from 2×10^{-3} to 0.5 Å^{-1}, corresponding to distances from ~ 2 to 3000 Å^{-1}.

On the other side, the structure of concentrated gels (volume fraction from 5×10^{-2} to 0.1 g/ml) was investigated using neutrons on PAXE, a small angle diffractometer of the Labratoire Léon Brillouin (LLB) in Paris.

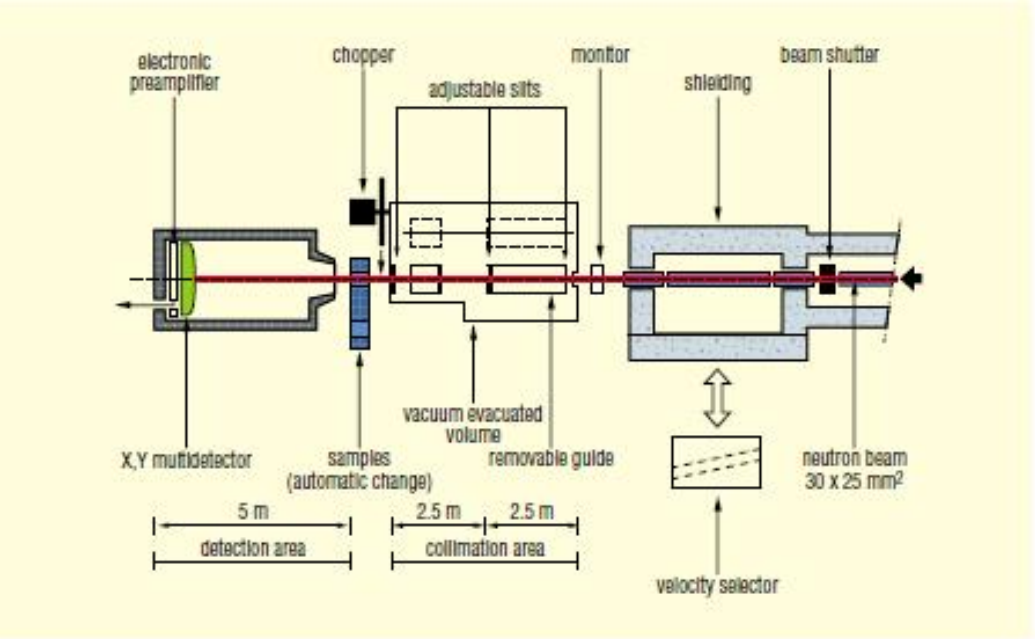

Figure 4.3: Scheme of PAXE taken from LLB website.

In this SANS experiment the instrumental resolution $\Delta\lambda/\lambda = \Delta E/E$ is between 5 and 15% depending on the experimental setup chosen. Varying the sample to detector distance and correspondingly the wavelength λ of the incident beam, we explored a Q-range from 4×10^{-3} to 4×10^{-1} Å^{-1}, corresponding to distances from 15 to 2000Å.

4.2.2 Data analysis

The general equation for absolute neutron scattering by macromolecules in solution combines the polymer form factor, indicated in the following as $P(Q)$, with the interparticle scattering factor[19,20], named $S_2(Q)$. The latter is the second term of the series expansion, at low Q, of the structure factor $S(Q)$ introduced in Chapter 2: $S_2(Q)$ reflects the interactions between the segments of two different chains ("pair term"). In the following equa-

tion, the "self" and "pair" particle contributions to the total intensity are evidenced:[19,20]

$$I(Q)(cm^{-1}) = \frac{1}{V}\frac{d\sigma}{d\Omega} = (\Delta\rho)^2(\varphi V_{chain}P(Q) + S_2(Q)) \tag{4.1}$$

$(\Delta\rho)^2 = (\rho_{HYA} - \rho_{D_2O})^2$ is the contrast factor per unit volume between polymer and solvent, to be determined from the known chemical composition. ρ= $\sum n_i b_i/(\sum m_i v/N_A)$ represents the scattering length per unit volume, b_i is the neutron scattering length of the species i, m_i the mass of species i, and v the specific volume of hyaluronan (0.59 cm^3/g) or D_2O. $V_{chain} = Nvm/N_A$ is the volume of the N monomers (of mass $m = 400$ g/mol each) in a chain and φ is the volume fraction of monomer and N_A the Avogadro's number.

The scattering intensity measured on concentrated gels, $\varphi > 8 \cdot 10^{-3}$ g/ml, has been described in terms of the sum of a dynamic and a static component[21–23]

$$I(Q) = I_{osm}(Q) + I_{stat}(Q) \tag{4.2}$$

in which

$$I_{osm}(Q) = \Delta\rho^2 \frac{kT\phi^2}{M_{osm}} \frac{1}{1 + Q^2\xi^2} \tag{4.3}$$

$\Delta\rho^2$ is the contrast factor between the solvent and the polymer, k is the Boltzmann constant and ξ is the thermal correlation length. M_{osm} is the longitudinal osmotic modulus of the gel, which in our analysis is a parameter of the fit. For neutral gels it is usually found that concentration fluctuations frozen-in by crosslinks cause extra scattering, $I_{stat}(Q)$, which is described by a Debye-Bueche structure factor[24]

$$I_{stat}(Q) = \Delta\rho^2 \frac{8\pi\Xi^3\langle\delta\varphi^2\rangle}{(1 + Q^2\Xi^2)^2} \tag{4.4}$$

Ξ is the correlation length of the frozen-in structure and $\langle \delta\varphi^2 \rangle$ is the mean square amplitude of the associated concentration fluctuations. In systems containing additional superstructures, such as aggregated domains or crystallites, $I_{stat}(Q)$ includes further terms, the functional form of which depends on the nature of the association.

4.2.3 Results and discussion

Since the gels were prepared in high ionic strength solutions, where intermolecular effects should be diminished, for diluted systems we assumed that the scattering arises from isolated chains i.e., $S_2(Q)$ in Equation 4.1 is equal to 0 and thus $I(Q) \propto P(Q)$.

The radius of gyration, R_g, an important parameter in the field of small angle scattering, is found from the so-called *Guinier approximation*, used to describe $I(Q)$ at low Q.[20] In our case, since HYA and HYADD have a high MW $\sim 10^6$, the Guinier region falls outside the measured Q range. To determine R_g one should perform light scattering experiments that allow to probe even lower Q.

In the case of diluted systems investigated with X-rays, a qualitative analysis through asymptotic expressions was sufficient to understand the structure of HYADD and HYA chains.

Figures 4.4 and 4.5 report the resulting scattering profiles obtained from samples of concentration between 0.3% and 0.8%.

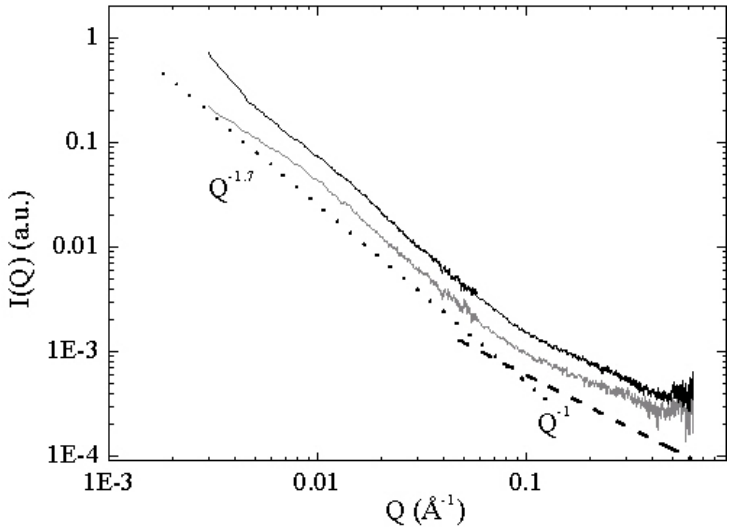

Figure 4.4: SAXS profiles of HYADD gels at 0.3% (gray line) and 0.5% (black line). The dotted and the dashed lines are guides to the eyes: their slopes are respectively $Q^{-1.7}$ and Q^{-1}.

The scattering intensity measured on HYADD diluted gels shows the presence of two distinct regions. At high wave vectors, i.e. $Q > 0.8$ Å^{-1}, one can observe a Q^{-1} decrease, typical of rod-like structures: in real space this means that HYADD chains remain almost rigid up to lengths of ~ 80 Å. Considering higher distances, i.e. lower Q, one starts to see bigger portions of chains: the slope of the scattering profiles in this region (see Figure 4.4) indicates that the polymer starts to organize like a random coil in which chains volume cannot be neglected; such a folding, in which excluded volume effects have to be considered, is called *self avoiding random walk* (SAW) and it is common for polymers of high molecular weight.[25] Our interpretation of the presented considerations is that the hexadecylic chains grafted on HYA main chains act like short external branches: they produce intramolecular interactions and the main chain can therefore interact with itself and curl up. The absence of the chemical modification is

clearly visible in SAXS profiles of natural HYA.

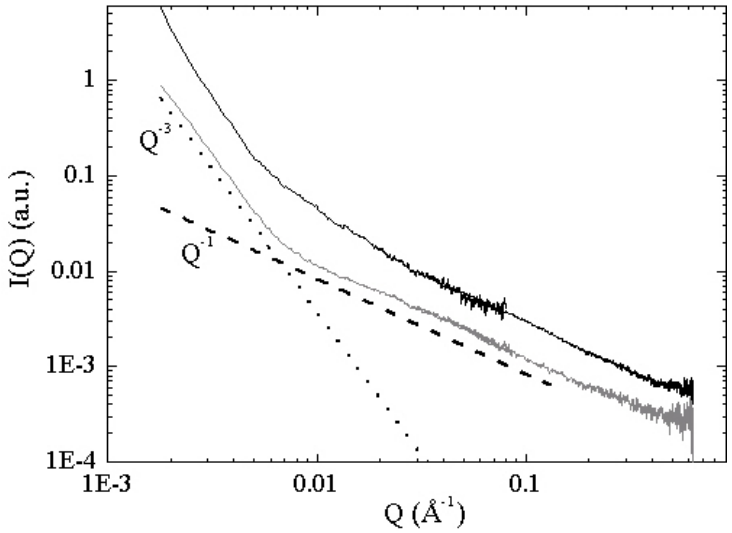

Figure 4.5: SAXS profiles of HYA solutions at 0.3% (gray line) and 0.8% (black line). The dotted and the dashed lines indicate respectively a Q^{-3} and a Q^{-1} slope.

From Figure 4.5 one can observe that HYA chains maintain their rigidity over distances much bigger than those of HYADD: the typical slope of rod structure ($I(Q) \propto Q^{-1}$) continues down to 0.007 Å^{-1}, corresponding to distances of almost 1000 Å. In the region of lower Q the slope increases abruptly ($I(Q) \propto Q^{-3}$) indicating the formation of three dimensional structures.

Increasing the concentration of polymer, the two kinds of hyaluronate continue to present significant differences.

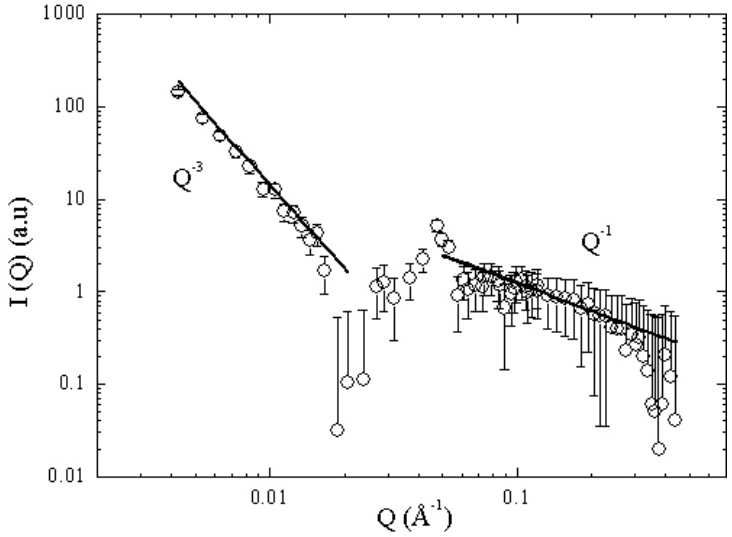

Figure 4.6: SANS profile of HYA gel of concentration 0.1 g/ml.

Figure 4.6 shows, as example, the SANS profile of HYA at 10%. In general, we discovered the scattering intensity of concentrated HYA gels to decrease with the same power laws as that of diluted samples. The difference between diluted and concentrated regime is that, in the latter, an evident structure peak shows up: for HYA gels of concentration 10% the peak is at $Q \sim 0.046$ Å^{-1}, i.e. $d \sim 137$ Å in the real space. With simple geometrical considerations, one obtains that, for bidimensional structures like rods, if the scatterers concentration is halved, the distance between the bidimensional scattering objects increases of a factor $\sqrt{2}$. In reciprocal space, i.e. the space normally considered in scattering experiments, the just mentioned ratio between peaks position has to be inverted: we expect therefore that for HYA gel at 5% the structure peak would be at a wave vector reduced of almost a factor $\sqrt{2}$ respect to the Q found for the gel at 10%. In Figure 4.7 the scattering profile of HYA 5% is reported: a vertical line marks the expected position of the structure peak at this concentration ($Q \sim 194$ Å^{-1}), knowing the peak position at 10%. Since HYA signal is low

for neutrons and the errors are significant, the peak for HYA 5% is not as pronounced as in the profile of the most concentrated gel; however, we can see that at the peak expected position, the noise in the profile increases as if there was a "hidden" peak.

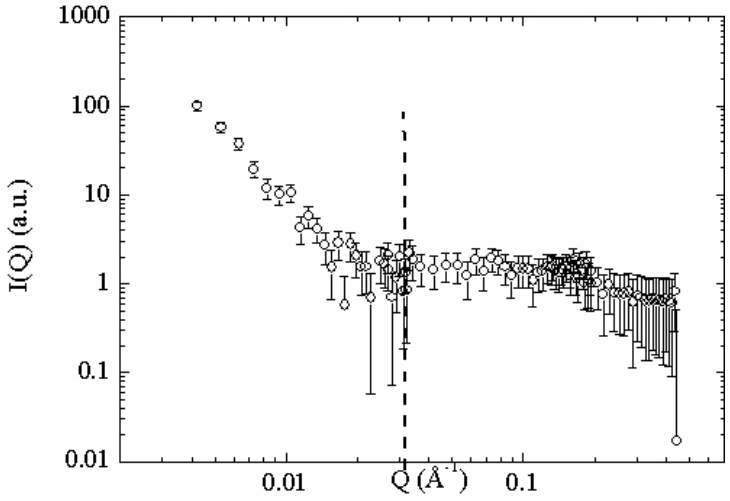

Figure 4.7: SANS profile of HYA gel of concentration 0.05 g/ml.The vertical dashed line indicated the position of the expected structure peak, i.e. $Q \sim 0.033\text{Å}^{-1}$.

Coming back to the profile of HYA at 10%, something more can be said about gel structure. Plotting, for clarity, SANS data without error bars, it appears that besides the clear peak already mentioned, one can distinguish other two smaller peaks : their positions, even if affected by quite big errors, are in the same ratios as those typical of an hexagonal organization, i.e. 1, 2 and $\sqrt{3}$.

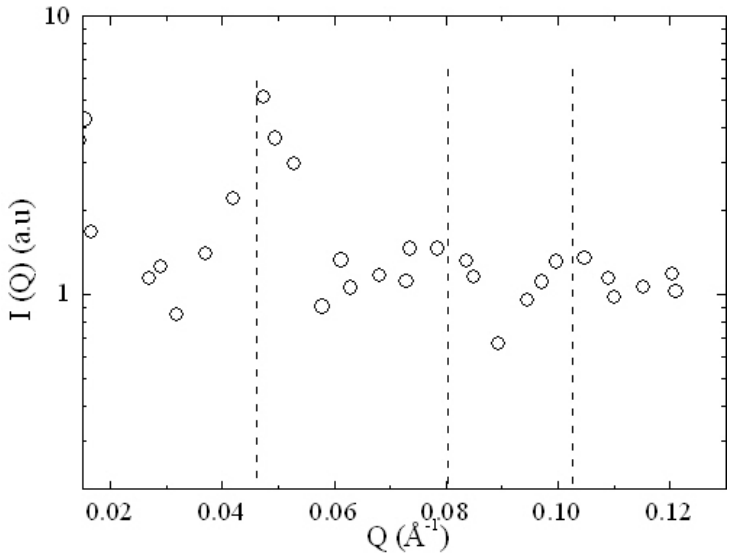

Figure 4.8: Zoom on the SANS profile of HYA gel at 0.1 g/ml, without error bars. The three dashed lines indicate the position of the three peaks: from left to right the first is at $Q \sim 0.046$ Å^{-1}, the second is at $Q \sim 0.078$ Å^{-1} and the last at $Q \sim 0.1$ Å^{-1}.

No structure is found, on the contrary, in concentrated HYADD gels. For these systems we considered the analytical model developed originally for cross-linked gels[21–23]. The chemical modification introduced in HYA to obtain HYADD does not create a chemical gels, since the peculiar gelification properties due to the presence of hexadecilic chains come always from hydrophobic interactions. The stability of the resulting physical gel, however, makes the model chosen (see Equation 4.2) reasonably appropriate.

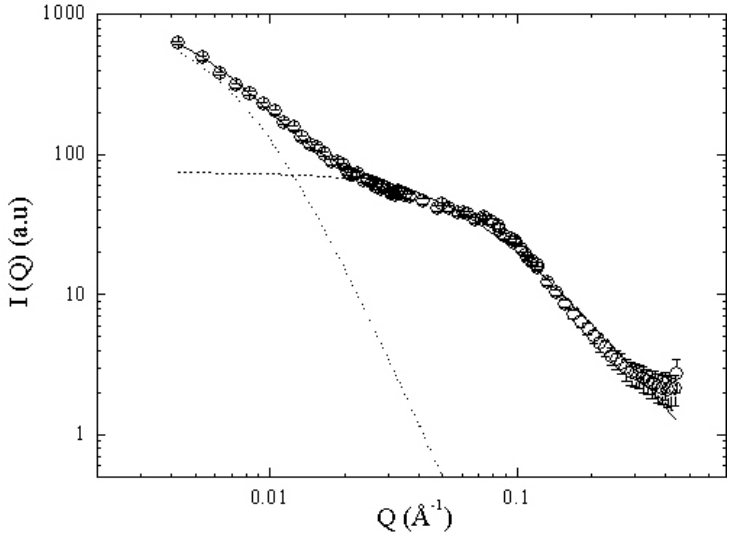

Figure 4.9: Scattering intensity of HYADD at 0.1 mg/ml. The dashed lines represent the static and dynamic contributions, at low and high Q respectively (see Equation 4.2)

The following table reports the correlation distances found for HYADD gels. Both lengths, ξ and Ξ, show a dependence upon concentration variation.

Table 4.1: Correlation lengths obtained fitting SANS profiles of HYADD gels to Equations 4.2, 4.3 and 4.4.

HYADD concentration	ξ (Å)	Ξ (Å)
1%	23 ± 2	191 ± 8
3%	19 ± 1	181 ± 8
5%	19 ± 1	127 ± 4
10%	14 ± 1	116 ± 4

4.3 Polymer dynamics

4.3.1 Elastic and quasi-elastic scattering experiments

The elastic neutron scattering experiment was performed on IN13 (see Chapter 3 for a complete description). We explored the temperature range between 280 and 320 K with steps of 10 K; high signal to noise ratio was obtained with acquisition runs of 5 hours. The elastic scattering intensity was corrected for the empty cell contribution and normalized to a slab vanadium standard, 2 mm thick; the data reduction was done using the ILL routine $LAMP$.

The quasi-elastic dynamics of the polymer chains was studied using SPHERES, a backscattering spectrometer located in the FRM II reactor in Munich.

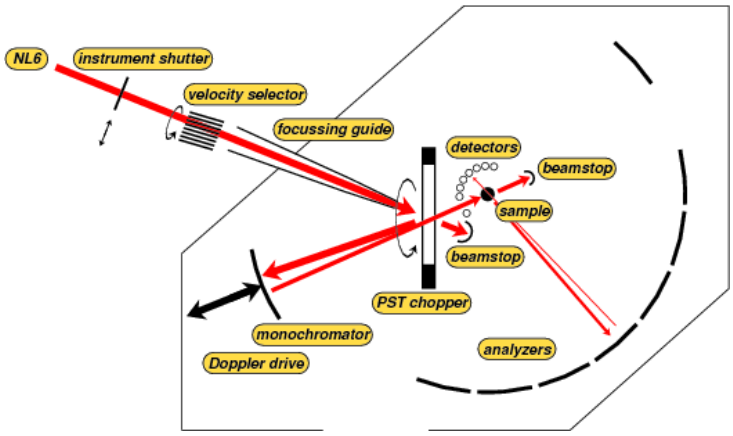

Figure 4.10: Layout of the high resolution backscattering spectrometer SPHERES.

Referring to Figure 4.10, it is easy to understand the functioning of the spectrometer. A mechanical velocity selector transmits a wavelength of 6.27 Å $\pm\, 6\%$. Neutrons enter the instrument housing through a convergent neutron guide, and reach the phase-transform chopper. If transmitted by

the chopper, neutrons are absorbed by the primary beam-stop, otherwise they are deflected by pyrolytic graphite (PG) crystals and sent towards the monochromator. After this deflection by crystals the wavelength band is compressed, while the spatial divergence is enhanced. The monochromator consists of highly ordered Si crystals. Only a small band of neutrons meets the Bragg condition under an angle of almost $180°$. The wavelength of these neutrons is modulated by the Doppler effect. To this purpose, the monochromator is mounted on a linear drive, which performs an oscillatory motion with up to 4.7 m/s. When neutrons fulfill the backscattering condition, they are sent back towards the chopper. In the meantime, the chopper rotor has moved by half a period so that the PG crystals are out of the way, allowing the neutrons to reach the sample. Neutrons that are scattered from the sample directly onto a detector are ignored by the data acquisition system. Useful neutrons are scattered from the sample towards the analyzers: from there, they are sent back to the detectors only if they fulfill again the backscattering condition. This is the events sequence if the scattering process within the sample is accompanied by an energy shift, which just compensates the energy shift caused by the Doppler effect in the oscillating monochromator.

4.3.2 Data analysis and results

The dynamics of polymer chains hydrogens was first investigated through IN13 experiment, in order to obtain information on hydrogens mean square displacement $\langle u^2 \rangle$. Figure 4.11 shows the elastic scattering intensity measured on HYADD gel of concentration 0.1 g/ml at different temperatures (see figure caption for details). HYADD gel of concentration 0.05 g/ml gives a similar result.

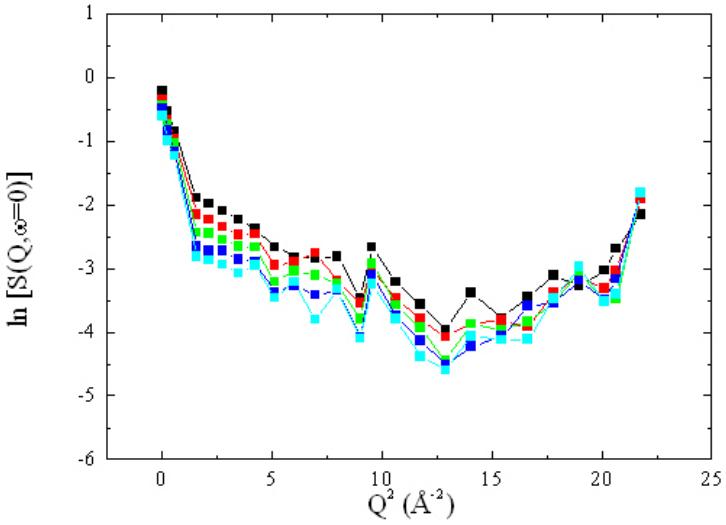

Figure 4.11: Elastic intensity measured on HYADD gel of concentration 0.1 g/ml (i.e. 10%), at different temperatures. *From top to bottom*: 280 (black), 290 (red), 300 (green), 310 (blue) and 320 K (light blue).

In the explored range, the elastic intensity is not strongly affected by temperature. For both polymers (HYADD and HYA) and both concentrations probed (10% and 5%), the intensity decrease in the low Q region, i.e. the PSD region where $Q < 1.2$ Å^{-1}(see IN13 description in Chapter 3), is very steep: the resulting mean square displacement values are significantly too high for the Gaussian approximation. The slope of the intensity decay decreases in the intermediate region of Q, i.e. for wave vectors between 1.2 and 2.1 Å^{-1}: here, if we do a linear fit of the logarithm of the intensity as a function of Q^2 (see Chapter 2 for the general equations), the resulting mean square displacement is temperature independent and has an average value of 0.52 ± 0.07 Å. The total absence of any $\langle u^2 \rangle$ variations with temperature basically indicates that the dynamics of the considered systems is too fast for the energy window chosen on IN13.

Since the count rate of IN13 was too low to perform a quasi-elastic ex-

periment in the beam time available, we carried out QENS measurements on SPHERES. The dynamics scattering function adopted to model the scattering of the gels on SPHERES can be written as follows:

$$S(Q,\omega) = exp(-\langle u^2 \rangle Q^2/3)[A_0(Q)\delta(\omega) + (1 - A_0)L(Q,\omega)] + B \qquad (4.5)$$

The first factor refers to the Debye-Waller factor (see Chapter 2), A_0 is the polymer EISF and $L(Q,\omega)$ is a lorentzian function. B is a flat background due to fast polymer motions, to water signal and, eventually, to instrumental characteristics. To fit the experimental spectra, Equation 4.5 was convoluted with the instrumental resolution. The fits were performed using a nonlinear minimization procedure based on MINUIT package.[26] In the energy range available on SPHERES and for the temperatures investigated, we assumed that the only quasi-elastic contribution to the scattering comes from polymer hydrogens slow motions; D_2O signal is indeed too large for the energies explored[27,28] and on SPHERES it appears therefore as a flat background.

We described the dynamics of HYADD and HYA protons in terms of an elastic component plus a quasi-elastic broadening: a single Lorentzian function results to be sufficient to obtain good fits of the QENS spectra. Figure 4.12 shows spectra of HYADD gel at 10 % measured at different temperatures, together with their fits to Equation 4.5; the spectra reported were taken at the same Q value, namely 0.6 Å^{-1}.

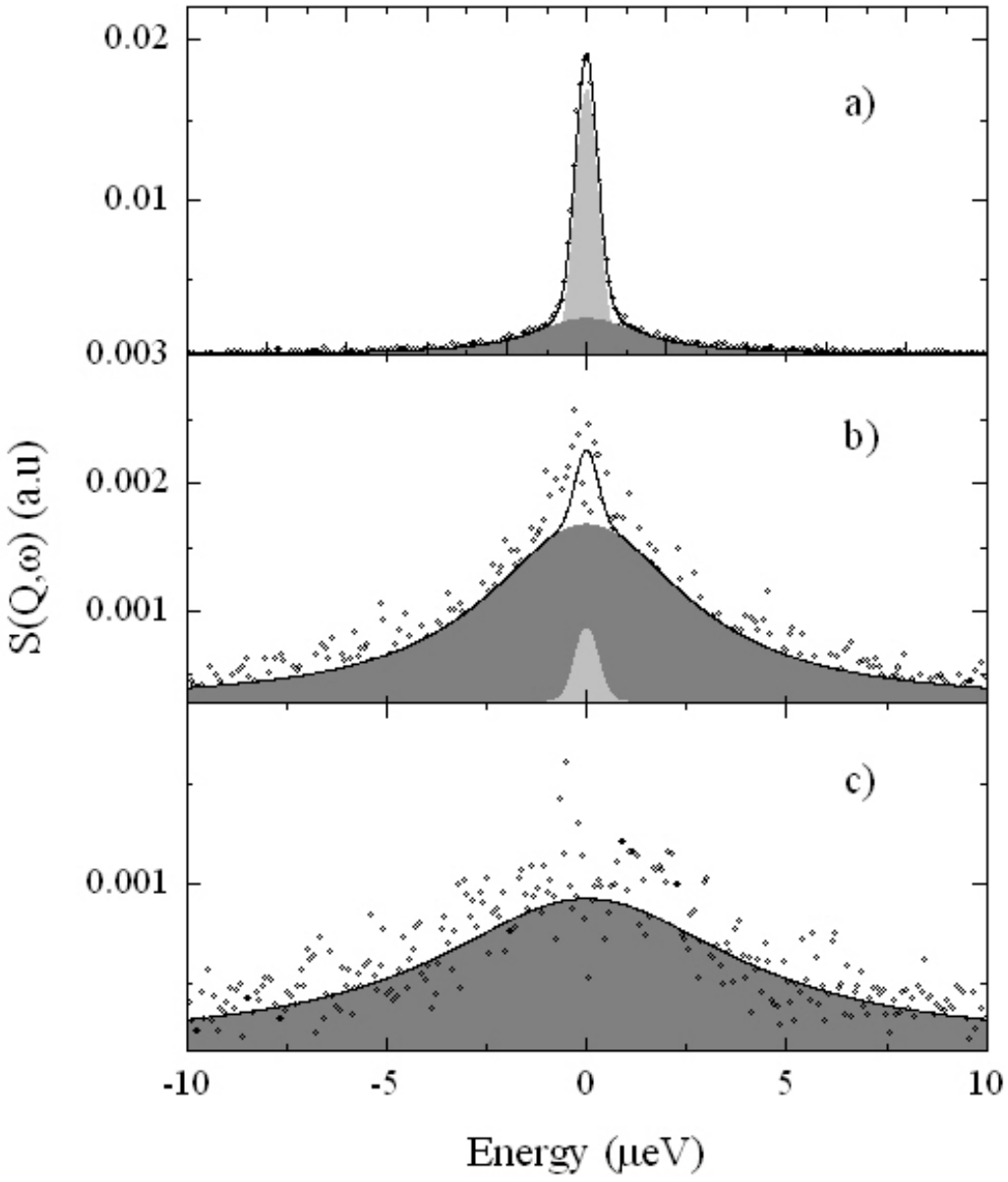

Figure 4.12: SPHERES spectra ($Q = 0,6$ Å^{-1}) of HYADD gel at 10%: 270 K (panel a), 280 K (panel b) and 300 K (panel c). In every frame the black line represents the total fit to Equation 4.5, the dark grey area indicates HYADD quasi-elastic contribution, while the light grey shadowing stands for the elastic contribution.

Both in HYADD and HYA gel, the mobility of polymer hydrogens depends significantly on temperature: the elastic component, well visible in the spectrum at 270K, shows a strong decrease in intensity at 280 K and it disappears completely at 300K. In the energy range probed on SPHERES, i.e. between -10 and $+10$ μeV, we see all the hydrogens moving at 300 K.

As already introduced in Chapter 2, the EISF parameter, A_0 in Equation 4.5, represents the Fourier transform of hydrogens confinement volume. Depending on the model chosen to fit it, we obtain information on the size of the confinement volume and on the kind of motions experienced by hydrogens inside it. Normally, in the EISF fit function, a background referring to the fraction of hydrogens seen as immobile by the particular machine used is also added.

Several paths were tried to interpret the trend of HYADD and HYA EISF as a function of Q: models such as the simple diffusion inside a sphere[29] or the jump among N sites[7] did not produce good fits. We decided therefore to consider, as confinement volume, a sphere with radius distributed according to a certain distribution function.

$$A_0(Q) = f + (1-f)\int C(r)\left[\frac{3j_1(Qr)}{Qr}\right]^2 \tag{4.6}$$

f represents the fraction of immobile protons, $j_1(Qr)$ is the first order Bessel function and $C(r)$ is the distribution function of the sphere radius, r. The distribution that turned out to be the most suitable to fit the EISF is the log-normal one. It can be written as

$$C(r;\mu,\sigma) = \frac{1}{r\sigma\sqrt{2\pi}}e^{-\frac{(ln(r)-\mu)^2}{2\sigma^2}} \tag{4.7}$$

μ and σ are the mean and standard deviation of the variable's natural logarithm (by definition of the log-normal distribution, the variable's logarithm is normally distributed). In our case r is the log-normally distributed

variable: its expected value (mean) can be derived from μ and σ:

$$\langle r \rangle = e^{\mu + \frac{1}{2}\sigma^2} \tag{4.8}$$

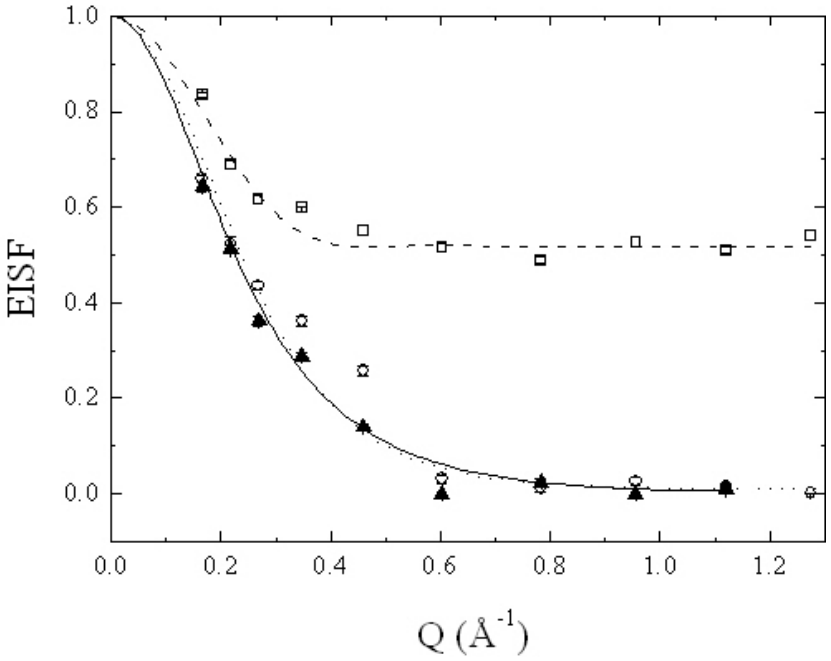

Figure 4.13: EISF of HYADD at 10% and its fit for each temperature probed: empty squares and dashed line refer to 270K, empty circles and dotted line to 280K and black triangles and continuous line refer to 300K.

Figure 4.13 presents the EISF parameter of HYADD gels at 10%, at the three temperatures considered; the fits were done to Equation 4.5. The lines in the figure are the fits of the EISF to Equation 4.6. In the following table we report the resulting parameters μ and σ describing the distribution and the calculated mean values of the radius of the confinement sphere.

Table 4.2: Parameters μ and σ of the log-normal distribution followed by the mean radius of the confinement sphere considered in HYADD gel.

Sample temperature (K)	μ	σ	**Mean radius** (Å)
270	2.2	0.20	9.6
280	2.0	0.37	8.1
300	2.1	0.47	8.9

In the above table the errors of the parameters are not reported to make the table more readable, however the uncertainty on the radius mean value results to be approximately 5% at every temperature: this means that there is not a clear trend in temperature for the radius of confinement; we assume therefore a unique value averaged over the three temperatures of 8.9 ± 0.4 Å. This value is far too big to be related to the motion of a single proton: more realistically it could be thought, for example, to represent the confined motion of a monosaccharide ring as a whole.

The quasi-elastic signal of the polymer was analyzed in terms of the half width at half maximum (HWHM), $\Gamma_{pol}(Q)$, of $L(Q, \omega)$, the Lorentzian function in Equation 4.5.

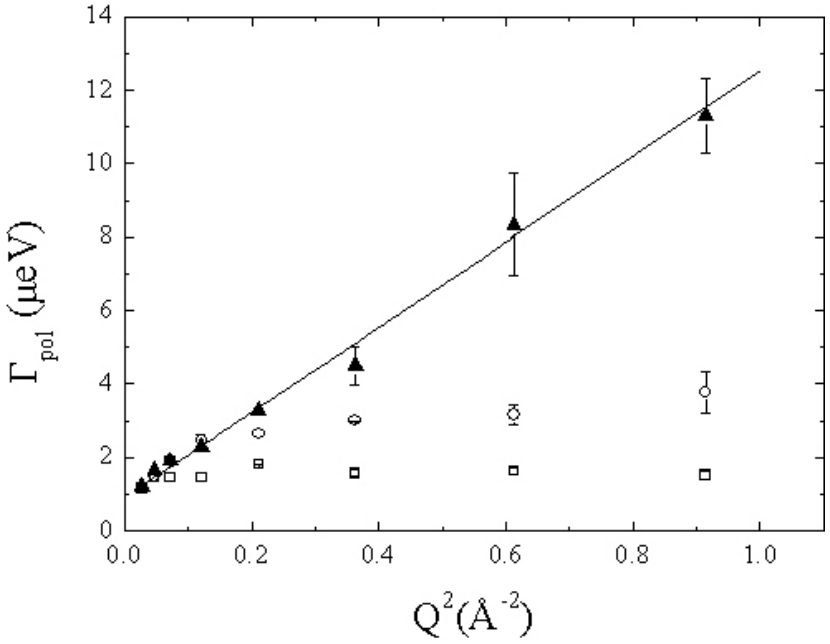

Figure 4.14: Q^2 dependance of Γ_{pol} found for HYADD gel at 10% at the three temperatures probed: 270K (empty squares), 280K (empty circles) and 300K (black triangles). The continuous line is a linear fit done on the widths at 300K.

At 270K the width of the Lorentzian is independent on the wave-vector, indicating localized motions. This behavior changes when rising up the temperature: at 280K there is an initial increase at low Q, that soon stops on a plateau at $Q^2 \sim 0.2$ Å^{-2} (i.e. $Q \sim 0.46$ Å^{-1}) ; such a trend could be assimilated to that of a random jump diffusion (for detailed explanations, see the following section and reference[30]); at 300K, the HWHM shows a linear increase as a function of Q^2, typical of a Fickian diffusion process: the diffusion coefficient found from a linear fit is $D_{HYADD} = (17.5 \pm 0.8)10^{-7}$cm^2/s. Apart from the parameter value, we need to answer to a question: what is this diffusion process related to? As mentioned to explain the results of the EISF fit, we think that the motion observed is related to the single sugar ring as a whole: at low temperature we see only the local rotations

around the main chain axis, while rising the temperature we start to see the diffusion related to the global motion of the chain.

4.4 Dynamics of water

4.4.1 QENS experiment

To probe water dynamics we used NEAT, the quasi-elastic spectrometer at the neutron source in Helmoltz Zentrum Berlin.

NEAT was set at an incident neutron wavelength of 6 Å (incident energy = 2.2 meV). The resulting energy resolution (full width at half maximum, FWHM) was 70μeV, and the explored Q-range between 0.3 and 1.6 Å^{-1}. The spectra were recorded in an energy range from -0.5 to 4 meV. With the adopted instrument configuration, motions on a time scales from 0.1 to 10 ps and on distances from about 4 to 20 Å can be investigated.

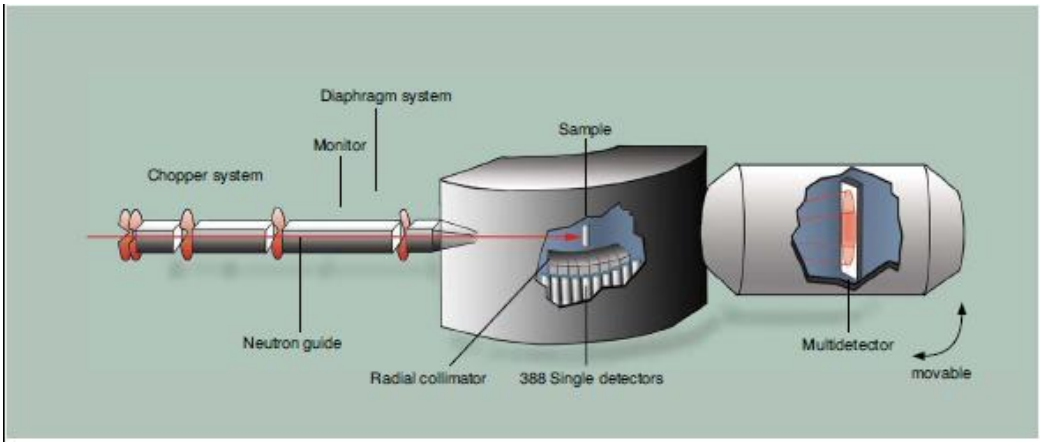

Figure 4.15: Drawing of NEAT.

Since the interest in such an experiment was onto the dynamics of water in the gels, HYA and HYADD samples were prepared in H_2O at con-

centrations from 1 to 10%. The measurements were performed at three temperatures: 285, 300 and 320 K.

4.4.2 Data analysis

The fitting function adopted to model NEAT gels spectra is made by an elastic component accounting for polymer contribution plus a quasi-elastic one representing water scattering function:

$$S(Q,\omega) = exp(-\langle u^2 \rangle Q^2) \left[p_{pol}\delta(\omega) + (1 - p_{pol}) S_{water}(Q,\omega) \right] \qquad (4.9)$$

$exp(-\langle u^2 \rangle Q^2)$ is the Debye-Waller factor accounting for the fast hydrogen mean square fluctuations, p_{HYA} is the relative weight of the biopolymer sub-spectrum and B is an instrumental background. Due to the high incoherent cross section of hydrogen and the low polymer concentration, p_{pol} reaches the maximum of 0.05 for the most concentrated gels, and the total signal is therefore dominated by water contribution. Moreover the low resolution of NEAT does not allow to distinguish between an elastic and a quasielastic contribution of the polymer: a single elastic signal is enough to represent polymer signal. Hereafter, examples of HYADD spectra measured at $Q = 1$ Å^{-1} are shown with their fits to Equation 4.9; each panel corresponds to one concentration.

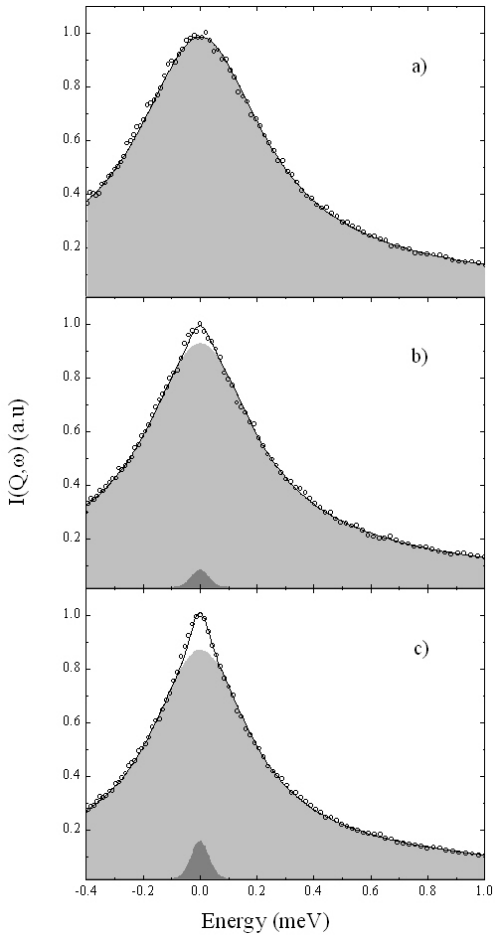

Figure 4.16: NEAT spectra of HYADD gels at the three different concentrations probed: (from top to bottom) 1%, 5% and 10%. The continuous lines are fits to Equation 4.9, the light grey areas represent water contribution while the dark shadowing stand for polymer elastic signal.

Solvent scattering function, $S_{water}(Q,\omega)$, musts take into account local rotational motions of water molecules as well as the long range translational diffusion that takes place following the breaking of the cage formed by the neighboring water molecules. The assumption of a decoupling between rotational and translational motions leads to a simple expression for S_{water}:

$$S_{water}(Q,\omega) = S_{trans}(Q,\omega) \otimes S_{rot}(Q,\omega) \tag{4.10}$$

In the past years this approximation has been debated and, in principle, it is a questionable approximation for an associated liquid like water whose structure is often depicted as that of an 'instant gel' dominated by H-bond interactions. However, it has been shown that, if the Q-values are far away from the maximum of the structure factor $S(Q)$ (i.e. $Q << 2$ Å^{-1}), the approximation works reasonably well at temperatures close to ambient and for characteristic times up to a few picoseconds.[31–33] These conditions are reasonably well matched in the present experiment, and we therefore applied the decoupling approximation.

For the translational component of Equation 4.10 we adopted the random jump model[30]:

$$S_{trans}(Q,\omega) = \frac{1}{\pi} \frac{\Gamma_{trans}(Q)}{\omega^2 + \Gamma_{trans}^2(Q)} \tag{4.11}$$

with a Q-dependent width of the Lorentzian profile, $\Gamma_{trans}(Q)$, given by:

$$\Gamma_{trans}(Q) = \frac{D_t Q^2}{1 + D_t Q^2 \tau_0} \tag{4.12}$$

where D_t is the self-diffusion coefficient and τ_0 denotes the residence time between consecutive jumps.

For the rotational component, $S_{rot}(Q,\omega)$, we compared two models: the first one is the classical isotropic rotation approach (see Sears[34]), while the second is a molecular jump mechanism of water reorientation, also called

'extended jump model' (EJM), recently proposed by Laage and Hynes;[35–37] It considers a two step process in which the rotation of the molecule implies bond breaking with an over-coordinated first shell neighbor and the formation of a new H-bond with an under-coordinated second-shell neighbor.

The expression of the rotational scattering function predicted by Sears model ca be written as

$$S_{rot}(Q,\omega) = \sum_l (2l+1) j_l^2(Qa) \frac{\Gamma_l(Q)}{\omega^2 + \Gamma_l^2(Q)} \tag{4.13}$$

where

$$\Gamma_l(Q) = \frac{1}{\tau_l} = l(l+1)\Gamma_{rot}(Q) \tag{4.14}$$

and τ_l is the characteristic rotational time, a is the O-H distance and $j_l(Qa)$ is the l-th order spherical Bessel function.

The EJM gives a expression of the linewidth Γ_l, in terms of a rotational jump time τ_{jump}, a jump amplitude $\Delta\theta$ and a frame rotational diffusion constant D_{frame}:

$$\Gamma_l(Q) = \frac{1}{\tau_l} = \frac{1}{\tau_{jump}} \left[1 - \frac{1}{2l+1} \cdot \frac{\left[\sin\left(l+\frac{1}{2}\right)\Delta\theta\right]}{\sin\frac{\Delta\theta}{2}} \right] + l(l+1)D_{frame} \tag{4.15}$$

4.4.3 Results and discussion

Let consider at first the analysis of the rotational motions: for both models, owing to the limited maximum scattering vector accessible ($Q_{max} \sim 1.8$ Å^{-1}), only the first two terms in the series expansion in Equation 4.10 contribute significantly to $S_{rot}(Q,\omega)$. Applying the Sears model, the obtained HWHM of the rotational Lorentzian is $\Gamma_1 = 350 \pm 50$ μeV, corresponding to a relaxation time $\tau_1 \sim 1.8$ ps: this value is in agreement to what is

reported in literature.[38] On the other hand, the fit of water rotational component with the EJM, gives a characteristic time very close to the Sears one: $\tau_1 \sim 1.5$ ps, coming from $D_{frame} \sim 3 \cdot 10^{-2}$ ps^{-1}, $\Delta\theta \sim 79°$ and $\tau_{jump} \sim 0.9$ ps. For the energy range explored on NEAT, the two models can be therefore considered equivalent .

Concerning water self-diffusivity, Figure 4.17 reports the values of $\Gamma_{trans}(Q)$ as a function of Q^2 resulting from the fit of HYADD spectra at 300K and at the three concentrations measured. In the graphic there is also an example of fit of the parameter to Equation 4.12. The same results are obtained for water long range diffusion in natural HYA gels.

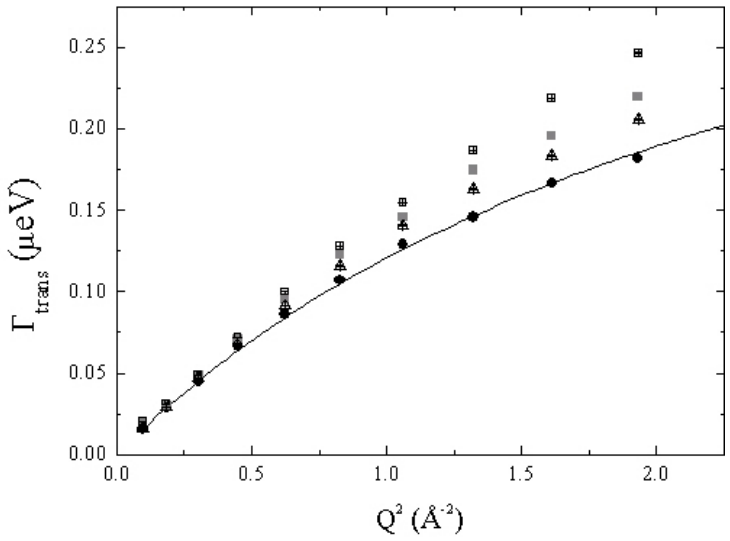

Figure 4.17: Values of $\Gamma_{trans}(Q)$ as a function of Q^2 for water in HYADD gels at 1% (black circles), 5% (open triangles) and 10% (open squares) and for bulk water (grey squares); the parameters refer to the measurements performed at 300 K. The continuous line is the fit of $\Gamma_{trans}(Q)$ for HYADD at 1% according to the random jump model.

As it is clear from $\Gamma_{trans}(Q)$ low-Q behavior shown in figure, water self-diffusion coefficient in HYADD gels, D_t, is very similar to that of bulk

water: for instance at 300K we can unify them under a unique mean value $D_t = (2.6 \pm 0.1) 10^{-5} \mathrm{cm}^2/\mathrm{s}$. In the following figure the values of D_t at every concentration are reported.

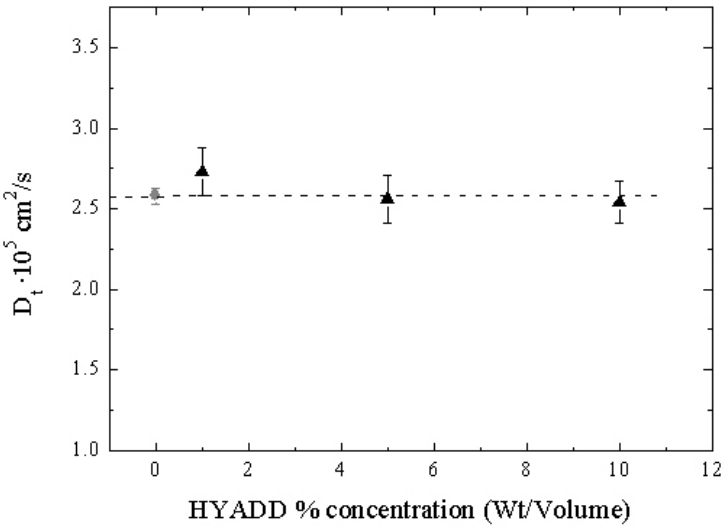

Figure 4.18: Self-diffusion coefficients for water in HYADD gels (black triangles) as a function of polymer concentration at 300K. The self-diffusion coefficient of bulk water at the same temperature is represented by the grey circle.

Changing the temperature, water keeps on showing the same dynamics in gels and in the bulk. The values of the micro-diffusivity coefficients of bulk water at different temperatures are taken from literature.[38]

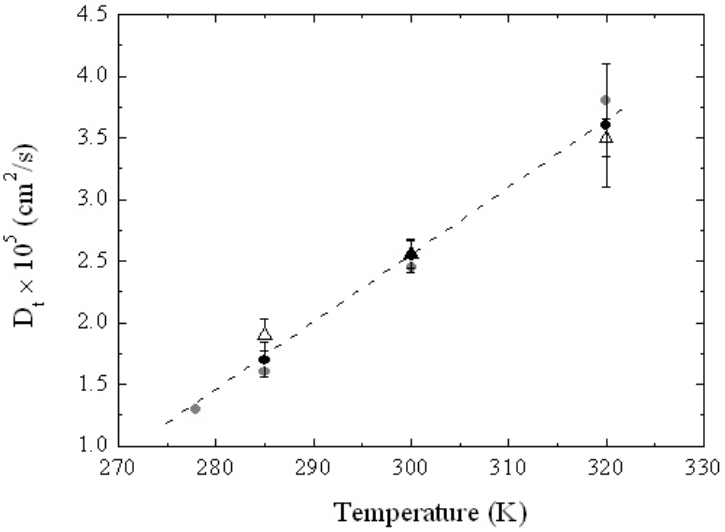

Figure 4.19: Values of the self-diffusion coefficients of water in HYADD gels at 1% (empty triangles) and 10% (black circles) as a function of temperature. The grey circles are the bulk water diffusion coefficients. The dashed line is a guide for the eye.

4.5 Conclusions

This section of the thesis focuses on the characterization of HYADD and HYA gels to investigate their structural properties on one side and, on the other, the dynamics both of polymer chains and of the solvent. To study the structure of the prepared gels as a function of polymer concentration we performed SAS experiments, in particular SAXS and SANS.

Respect to natural HYA gel, the presence of the chemical modification introduced to synthesize HYADD induces appreciable differences in gel structure.

The analysis of the diluted samples, i.e. of concentration from 0.3 to 0.8%, showed that HYADD chains have a rod-like form factor up to a chain

length ~ 80 Å, whereas the chains of the natural polysaccharide maintain this kind of structure up to ~ 1000 Å. In HYADD, the presence of the lateral hexadecylic chains along the backbone induces a coiling of the polymer: the power law describing the decrease in the scattering intensity as a function of Q ($I(Q) \propto Q^{-1.7}$, see Figure 4.4) indicates a self avoiding random walk: the chains coil up but, since their dimensions cannot be neglected, they cannot pass twice on the same point. Different is the behavior of HYA chains that aggregate in a surface fractal.

If the SANS intensity of both diluted and concentrated HYA gels could be analyzed in an asymptotic way, for HYADD samples we chose a model already used for cross-linked gels. In our case the gelification process is physical, the chains interactions come from hydrophobic effect and no covalent bonds are formed, however the model chosen fits well HYADD scattering profiles: we can therefore deduce than the fitting model for chemical gels remains valid also for 'stable' physical gels. In this framework we deduced a correlation length related to thermodynamics fluctuations and another one related to stable links formed between the chains. The latter correlation length, indicating the extension of density domains, decreases when increasing the concentration, showing how HYADD gel becomes less homogeneous when increasing polymer concentration.

In literature other works exist on the structure of native hyaluronate,[39,40] however, to our knowledge, the polymers there considered have a lower molecular weight than that of the hyaluronate considered in this thesis or the systems presented have lower concentrations than ours. Considering all the uncertainties related to the low neutron scattering produced by our gels, we found that HYA chains maintain a rod-like form factor from the most diluted to the most concentrated samples and when the chains start to 'feel' each other, an hexagonal organization appears between HYA chains. HYADD scattering profiles do not show such an architecture be-

cause probably the small arms grafted on HYA main chain induce intra-chain interactions and macroscopic domains appear.

The dynamics of polymer chains was probed with a high resolution backscattering spectrometer allowing to be sensitive to slow motions of characteristic times up to 1 ns. We saw that temperatures plays an important role in switching on and off polymer hydrogens motions. At 270 K protons have only local, non dispersive motions while a diffusion clearly appears at 300 K. This kind of motion could be interpreted as, for instance, a flip-flop motion between adjacent sugar rings. However to deepen and better characterize such a dynamics we recently performed a spin-echo experiment on IN15 at ILL, to be able to study slower motions.

The last element considered in this global understanding of HYADD and HYA gels was the dynamics of water in the systems: water turned out to move as in the bulk state, independently from polymer concentration and temperature. This is possible only because the samples were prepared in high ionic strength, meaning that the charges present all along the polymer chain are balanced by the ions in the solvent. In the gels probed therefore there is no interaction between sugar and water and the latter can move inside the loose polymer meshes as it does in the bulk state.

Chapter 5

Transdermal patches

In the last two decades a lot of interest has been devoted to the study of the diffusion of water and/or small molecules through biofilms.[41–43] A detailed knowledge of these processes at the molecular level is very relevant for instance to optimize the transport of nutrients or the process of drug delivery. Modern drug delivery focuses on 'versatile' carrier systems able to handle different types of drugs and of performing different release programs. In this framework, transdermal patch systems represent a technology with enhanced performances with respect to conventional drug administration routes providing significant clinical benefits over other dosage forms. Today patches are prepared with a typical multilayer structure usually formed by a support or backing layer, a drug reservoir, an adhesive and a protective layer to be removed before patch application. With the aim of simplifying the patch formulation and improving its performances, a novel design of transdermal platform, called Patch-non-Patch®[2,3], has been proposed. The Patch-non-Patch® system is a monolaminated bioadhesive film in which the usual constituents of transdermal patches (backing, drug and adhesive) are condensed in a single layer. Several active molecules have already been included in this film

such as, for instance, caffeine, ibuprofen, lysine, lidocaine, nicotine and progesterone.[2,5,6,44–46] In the present paper the focus is on lidocaine, a molecule commonly used as a local anaesthetic and anti-arrhythmic.

In transdermal films water plays a crucial role in terms of the adhesion[4] and of the release kinetics of the drug inserted. A Patch-non-Patch® is not self-adhesive in the dry state due to the small amount of adhesive present in the formulation, but adhesiveness is restored in presence of water on the skin surface where the patch is applied. The film then absorbs water, swells and the drug release can finally take place. The diffusivity of lidocaine through the polymer film here investigated, has been already studied by macroscopic permeation experiments[5]: it has been shown that the permeation profiles are not linear with time, but they typically show a fast initial permeation, followed by a reduced flux. The permeation data become linear when plotted versus the square root of time suggesting a matrix-type control of drug delivery by the film according to its hydration level.[6] With QENS, we probed the diffusivity, at a molecular level, of water and of drug molecules through the film in order to obtain information relevant to tailor the physical and chemical characteristics of the film for specific delivery programs.

5.1 Experimental

5.1.1 Sample preparation

The transdermal patches for the delivery of lidocaine were prepared by the group of Prof. Santi at the Department of Pharmacology of University of Parma.

The starting components for the film preparation are Polyvinylalcohol (PVA) MW: 83400, degree of hydrolysis 87%, Eudragit® E 100, a dimethy-

laminoethyl methacrylate polymer widely used in controlled drug delivery, lauric acid, adipic acid, glycerol and sorbitol. The adhesive component of the film, Plastoid® E 35 H, was prepared according to the protocol of Rofarma: Eudragit® E 100 (15.9 %, wt/wt), lauric acid (9.2 %, wt/wt) and adipic acid (1.8 %, wt/wt) were added to hot water (72.1 %, wt/wt, temperature $\sim$ 80 °C). The mixture was stirred, maintaining the temperature at $\sim$ 80 °C, until a clear solution was formed. The solution was then cooled to 60 °C and glycerol (1.0 %, w/w,) was added. The mixture was then gradually cooled to room temperature while stirring. All others chemicals were of analytical grade.

The adopted drug was lidocaine, provided as lidocaine hydrocloride (see Figure 5.1).

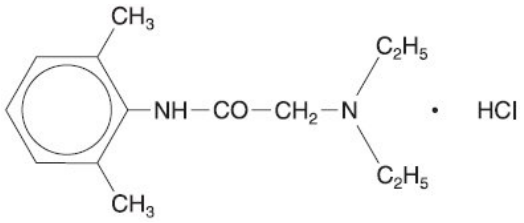

Figure 5.1: Molecular structure of lidocaine hydrocloride molecule.

The 'empty' film patches were prepared using a lamination technique. A water solution of PVA (20 % wt/wt) and the adhesive Plastoid® E 35 H were mixed in a $2:1$ ratio. The obtained mixture was magnetically stirred overnight and then laminated on siliconized paper. The film was dried in an oven at 80 °C for 30 minutes. The average thickness of the dried films was $115 \pm 15 \mu$m. The macroscopic physical properties of the patches have been described in literature.[47] The 'empty' film patches were used to investigate the dynamics of the 'pure' matrix. Films loaded with lidocaine were then prepared with the same procedure adding a lidocaine HCl solution in water/sorbitol to the pure film forming agent. To determine the

amount of lidocaine, circles of film, 0.6 cm^2 of area, were dissolved in 10 ml of distilled water. The solutions obtained were analyzed by HPLC. The final content of lidocaine was 2.7 ± 0.3 mg/cm^2.

Samples without lidocaine were prepared with the same procedure; they were used to investigate the dynamics of the 'pure' film matrix. The samples for the QENS experiment were hydrated with known amounts of either H_2O or D_2O up to a specific hydration level, h, (weight of water / total weight of the hydrated sample). In the text, the samples are labeled as follows:

- PHxx: samples without lidocaine in hydrogenous buffer
- PDxx: samples without lidocaine in deuterated buffer
- LHxx: samples containing lidocaine in hydrogenous buffer
- LDxx: samples containing lidocaine in deuterated buffer

5.1.2 QENS experiment

The QENS experiment has been performed using the ILL high precision direct geometry time-of-flight spectrometer IN5.

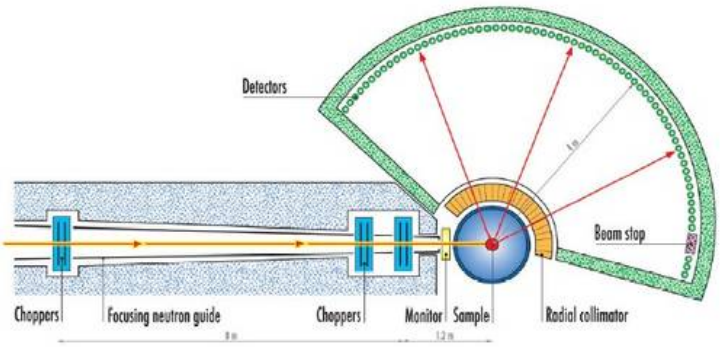

Figure 5.2: Layout of the IN5 spectrometer (image taken from IN5 website).

The instrumental configuration adopted for the experiment was characterized by an incident wavelength of 10 Å, giving a resolution of 15μeV (full width half maximum, FWHM) and a Q-range from 0.2 to 1 Å^{-1}. All the measurements were performed at room temperature keeping the hydrated samples in vacuum tight flat-geometry aluminium containers (size $30 \times 50 \times 0.3$ mm^3). Typical measuring times were around 3 hrs/sample. In order to carry out standard corrections, vanadium and pure water runs were also performed; using LAMP, an ILL suite of routines, we performed cell subtraction, self-shielding corrections, normalization and a first-order multiple scattering correction based on the geometry and transmission of the sample. The spectra were fitted in the energy range from -0.15 to 1.4 meV.

5.2 Data analysis

A cause of the complexity of the system studied, the analysis has been carried on through different steps. In order to first describe the scattering signal of the polymer matrix, the PD patch at low hydration have been analyzed at first: in the spectra of this sample the dominant contribution is

that of the polymer and it has been modeled using the scattering function:

$$S_m(Q,\omega) = \exp(-Q^2\langle u^2\rangle)\left[A_{0m}(Q)\delta(\omega) + (1 - A_{0m}(Q)) \cdot C_m(Q,\omega)\right] \quad (5.1)$$

$A_{0m}(Q)$ is the EISF attributed to protons of the matrix. The quasi-elastic term $C_m(Q,\omega)$, representing the dynamics of the polymeric matrix, has been described by a log-normal distribution of Lorentzian curves in the ω-domain, i.e. single exponential relaxations in the time domain:

$$C_m(Q,\omega) = \int G\left(\Gamma,\mu,\sigma\right)\frac{\Gamma}{\pi\left(\omega^2+\Gamma^2\right)}d\Gamma \quad (5.2)$$

where $G\left(\Gamma,\mu,\sigma\right)$ is the log-normal width distribution, μ is the average value of the $log(\Gamma)$ normal distribution, and σ is the standard deviation. The choice of a distribution of relaxation times for the quasi-elastic component is quite common in complex polymer systems and it is due to the heterogeneous environment of the hydrogens.[48] In our case, preliminary fits indicated that a log-normal distribution could reproduce the scattering profiles with better accuracy than a symmetric normal distribution.

In analyzing QENS data it is usually assumed that motions with markedly different timescales are decoupled (see Chapter 2). Therefore, in describing the dynamics of a complex polymer network at the atomic scale, fast (fs timescale) vibrational motions are assumed as independent from slower motions arising from conformational and/or diffusive dynamics (ps to ns timescale). Vibrational contribution is taken into account by an overall Debye-Waller factor $DW = exp(-Q^2\langle u^2\rangle)$, where $\langle u^2\rangle$ is the mean square atomic fluctuation. In the present analysis this fast contribution has been considered to be the same for all the different component of the system.

The second step in the data analysis consisted in considering patches with higher hydration level: from the samples in D_2O we investigated the dynamics of the polymer matrix as a function of hydration, and from the

H_2O ones we checked the behavior of water. The scattering contribution of the solvent has been represented by a simplified model made up by the weighted sum of two Lorentzian components $L_1(Q,\omega)$ and $L_2(Q,\omega)$:

$$S_w(Q,\omega) = \exp(-Q^2\langle u^2\rangle)\,[B(Q)L_1(Q,\omega) + (1 - B(Q))\,L_2(Q,\omega)] \quad (5.3)$$

This simplified scattering function has been adopted since the main interest of the study on such a system was focused on the diffusivity of lidocaine and we therefore neglected the dynamics detail of water, already well described in literature. While $L_2(Q,\omega)$ summarizes the fast local motions of a water molecule, in our context the most important aspect of the solvent behavior is its diffusivity, that can be derived by the Q-dependence of the first Lorentzian $L_1(Q,\omega)$. Its line shape has been described by a continuous distribution of random jumps, as we did in the analysis of hyaluronic acid based hydrogels (see Chapter 4); for the sake of clarity it is worth to rewrite the random jump expression:

$$\Gamma_t(Q) = \frac{D_t Q^2}{1 + \tau D_t Q^2} \quad (5.4)$$

where D_t is a microscopic diffusion coefficient and τ is the residence time between successive jumps.

Finally the spectra of the samples containing lidocaine were analyzed keeping fixed the parameters previously found for the polymer mixture and for water. For the internal dynamics of lidocaine molecules, a simplified version of the model adopted for the polymer matrix was considered replacing the log-normal distribution (equation 5.2) with a single Lorentzian curve, $L_l(Q,\omega)$ which describes therefore the average hydrogen dynamics. The lidocaine scattering function, $S_l(Q,\omega)$, is then written as:

$$S_l(Q,\omega) = \exp(-Q^2\langle u^2\rangle)\,[A_{0l}(Q)\cdot\delta(\omega) + (1 - A_{0l})\cdot L_l(Q,\omega)] \quad (5.5)$$

$A_{0l}(Q)$ represents the lidocaine EISF.

Analysing the hydrated patches loaded with the drug we described the motion of the lidocaine molecule as a whole, within the matrix+water system, in terms of Brownian dynamics: the resulting microscopic diffusion coefficient follows Fick's law. the resulting lidocaine scattering function, $S'_l(Q,\omega)$, is the convolution of Equation 5.5 with a Lorentzian function $L_{diff}(Q,\omega)$ which accounts for the Brownian diffusion of lidocaine:

$$S'_l(Q,\omega) = \exp(-Q^2\langle u^2\rangle)\left[A_{0l}(Q)\cdot\delta(\omega) + (1-A_{0l})\cdot L_l(Q,\omega)\right] \otimes L_{diff}(Q,\omega) \tag{5.6}$$

The total scattering function used to fit the patches spectra is then the weighted sum of the contributions of Equations 5.1,5.3 and 5.6 convoluted with the instrument resolution $R(Q,\omega)$ obtained from the Vanadium calibration run:

$$\begin{aligned} S_{total}(Q,\omega) = \exp(-Q^2\langle u^2\rangle)\{p\left[p_m S_m(Q,\omega) + (1-p_m)S_w(Q,\omega)\right] \\ +(1-p)\left[S_l(Q,\omega)\otimes L_{diff}(Q,\omega)\right]\} \otimes R(Q,\omega) \end{aligned} \tag{5.7}$$

p_m represents the relative weight of the polymer matrix subspectrum in the total patch contribution (polymer film + hydration water); p represents the relative weight of the hydrated patch subspectrum in the total QENS spectrum (patch + lidocaine). The p and p_m parameters have been determined on the basis of the sample compositions and of the neutron scattering cross-sections: they have been kept fixed in the fit procedures. It is worth mentioning that at the highest hydration investigated (h = 0.6) the weight of the matrix subspectrum p_m is 0.44 for the hydrogenous samples and 0.86 for those with deuterated solvent. Therefore in all the samples with D_2O the scattering cross section is dominated by the polymer contribution. These samples enabled us to determine with good accuracy the

parameters of the film and of lidocaine, while the H_2O-hydrated samples were used to determine the parameters related to hydration water. The total dynamic structure factor $S_{total}(Q,\omega)$ (Equation 5.7) contains several free parameters. They cannot be unambiguously optimized in a single fit procedure. The optimization process was performed in steps in order to handle a limited number of free parameters in each step. The first step was the analysis of the 'empty' patches. From the fit of the lowest hydration samples (h = 0.15) the parameters related to the polymer film were obtained, namely the EISF of the polymer, $A_{0m}(Q)$, and the parameters μ and σ of the log-normal distribution. The spectra of the patches with higher H_2O-hydration were then considered and the parameters of the water subspectrum were derived ($B(Q)$ and the widths Γ_1 and Γ_2 of the two Lorentzians in equation 5.3). The data of the lidocaine 'loaded' samples were analyzed following an analogous sequence. At first the lowest hydration samples were considered and the parameters of the lidocaine subspectrum ($A_{0l}(Q)$ and Γ_l) were determined, while keeping those of the polymer film equal to those obtained from the empty patches. Finally, the analysis of the hydrated 'loaded' patches provided the diffusion coefficient of lidocaine through the polymer film. The fits were performed using a nonlinear minimization procedure based on the MINUIT package.[26]

5.3 Results and discussions

The mean square fluctuation, $\langle u^2 \rangle$, in Equation 5.7 was assumed to have a common value for all the hydrogens in the sample. Its value can be derived from the Q-dependence of the total area of the scattering curve. The fits of the spectra gave $\langle u^2 \rangle = 0.15 \pm 0.03$ Å^2. This value is almost independent from hydration and it is close to that of pure water (0.18 Å^2).[27]

5.3.1 Dynamics of empty patches

The dynamics of the polymer matrix has been investigated starting from the spectra of the PD samples. Owing to the much lower cross section of deuterium with respect to hydrogen, for the most hydrated PD patches (h = 0.6), the scattering contribution of the matrix is 86 % of the total one. Figure 5.3 shows the comparison between the scattering profiles, taken at $Q = 1.02$ Å^{-1}, of the patches prepared in H_2O and D_2O with hydration h = 0.15. The two curves coincide within the experimental accuracy.

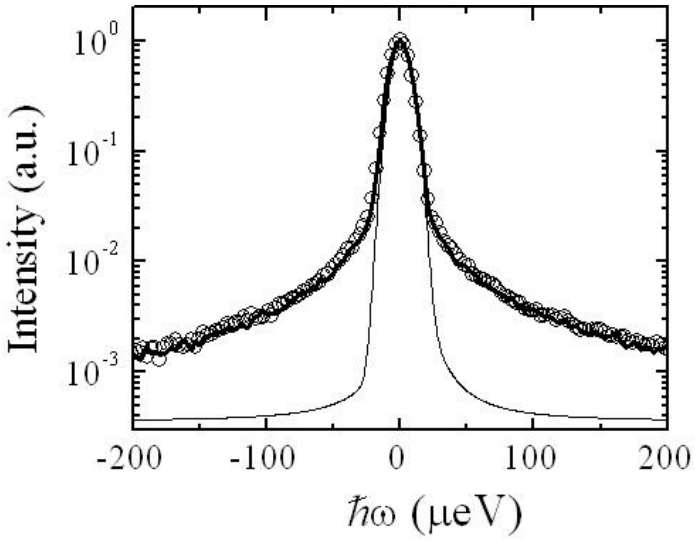

Figure 5.3: Normalized spectra of patches with hydration h = 0.15 at $Q = 1.02$ Å^{-1}: H_2O hydration, PH15 sample (open symbols), D_2O hydration, PD15 sample (heavy continuous line). The thin continuous line shows the measured instrumental resolution.

The relative weight of water contribution to the total scattering intensity is 14% for PH15 and only 2% for PD15. In the latter case therefore the signal is therefore almost totally due to the polymer matrix. From the comparison we can conclude that up to $h\sim$ 0.15, hydration water is closely

associated to the polymer matrix: no long range diffusion occurs and the dynamics of water coincides with that of the matrix. As an example, in Figure 5.4a, it is shown the spectrum of a PD15 sample at $Q = 1$ Å^{-1} fitted according to Equation 5.1: the elastic and quasi-elastic components are evidenced in the figure.

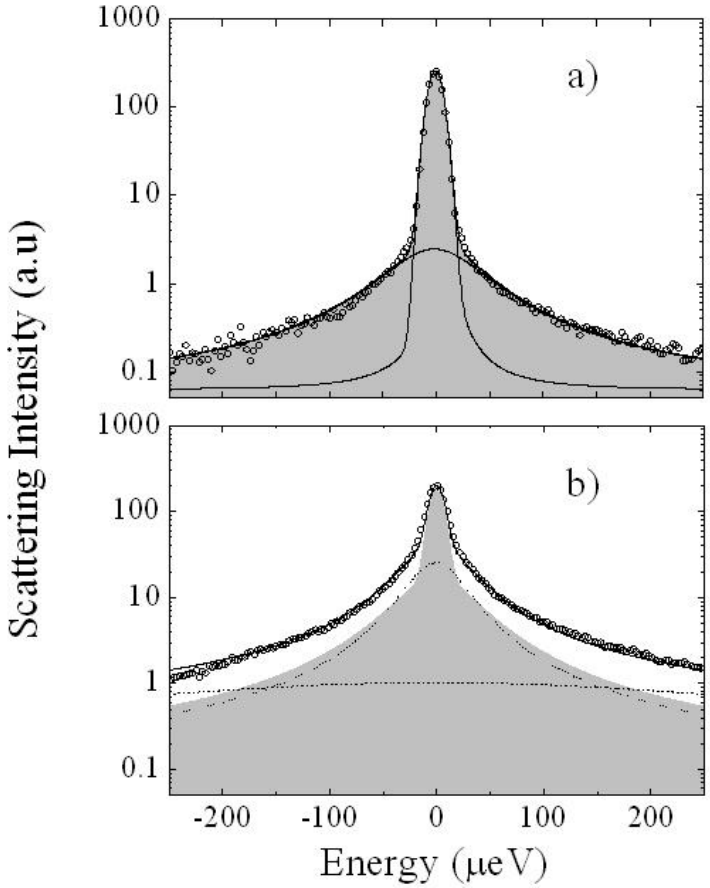

Figure 5.4: QENS spectra at $Q = 0.6$ Å^{-1} of: a) a PH15 sample. The elastic and inelastic components resulting from the fit are shown. b) a PH60 sample. The two dashed lines are the components (Lorentzian curves) due to mobile water (equation 5.3); the light gray area represents the total polymer contribution.

In Figure 5.4b it can be seen that a component much broader than that

of the polymer matrix shows up when hydration is increased. This component can be attributed to additional water that has a weaker association to the polymer and shows then a typical liquid-like behavior. Previous studies of hydration water in bio-gel systems evidenced that even if a fraction of water molecules is trapped within the gel junction zones, most of hydration water behaves in a way similar to that of bulk water.[49,50] Figure 5.5 reports the Q-dependence of the EISF, $A_{0m}(Q)$, of the polymer matrix for three different hydrations. The curves have been fitted assuming free diffusion within a spherical volume according to ref.[29]:

$$A_{0m}(Q) = f + (1 - f) \left[\frac{3j_1(Qr)}{Qr} \right]^2 \tag{5.8}$$

where f represents the fraction of protons that do not take part to the confined diffusion, $j_1(Qr)$ is the first-order spherical Bessel function, and r is the radius of the sphere that defines the confinement volume.

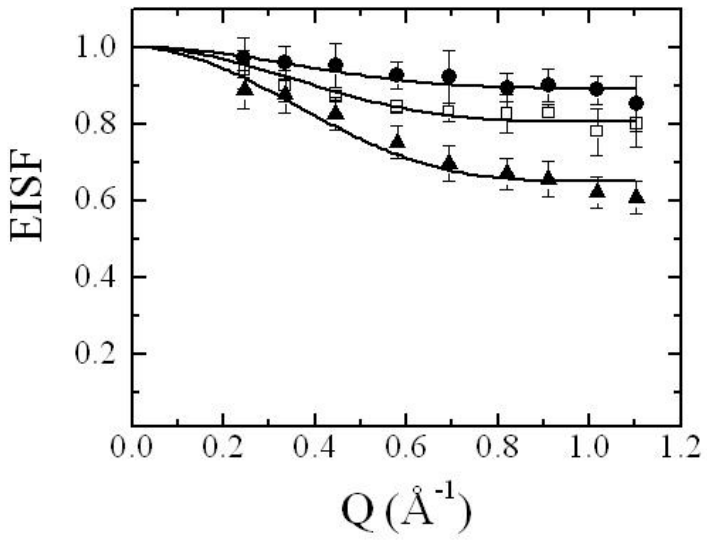

Figure 5.5: Q-dependence of the EISF, $A_{0m}(Q)$, of the polymer matrix for PD samples at different hydrations: (h = 0.15 ( ), 0.40 ( ), 0.60 (p)). The curves are fits to equation **??**.

The confinement radius r results almost hydration independent with average value 4.6 $\pm$ 0.7 Å. This value has been kept fix in the subsequent fits on the lidocaine-loaded patches (LD and LH samples). On the other hand, the fraction f decreases with increasing hydration. This indicates that an increasing number of hydrogens takes part to the confined diffusive motions. As explained in the previous section, the quasielastic component due to the polymer matrix has been described by a log-normal distribution of Lorentzians of average width $\langle\Gamma_Q\rangle$ = 46 μeV and standard deviation σ = 4. These values are not significantly affected by hydration. In addition, no appreciable Q-dependence of $\langle\Gamma_Q\rangle$ is observed in the Q-range explored (Q_{max} = 1.3 Å^{-1}). This confirms the local nature of the polymer motions in the time and space windows probed by the experiment.

5.3.2 Dynamics of hydration water

As previously remarked, the spectra of samples at $h > 0.15$ can be interpreted adding a further broad component to the spectra of low hydration samples (Figure 5.4b). This component has been attributed to 'mobile' water, and it has been described in terms of two Lorentzian curves (Equation 5.3). This model, known to be simplified and phenomenological, has already been used in describing the dynamics of bulk water[31] and of water interacting with other molecular systems.[51] The microdiffusivity parameters, D_t and tau_0 in equation 5.4 can be obtained analyzing the Q-dependence of the narrowest Lorentzian, $L_1(Q, \omega)$. Figure 5.6 shows the hydration dependence of these parameters: the slowing effect of the matrix on the diffusion of water is similar to that observed on different bio-films obtained with pulsed field gradient NMR.[43]

5.3.3 Dynamics of Lidocaine

The lidocaine contribution is clearly visible in the spectra of "loaded" samples since lidocaine represents about 30% of the total weight of dry patches. As an example, the spectra of the samples PD60 and LD50 are shown in Figure 5.7 at Q = 0.44 Å^{-1}. These two samples have similar values of the w water/ w polymer matrix ratio.

In the fit of the LH and LD spectra, the water and polymer matrix parameters were fixed to the values obtained for the 'empty' patches (PH and PD samples) with similar water content. Thus in these fits only the lidocaine parameters were varied. As already remarked, at low hydration ($h < 0.15$) water molecules are closely associated to the polymer matrix and no long range diffusion is observed. In such conditions lidocaine can not diffuse through the matrix as well. Its subspectrum has then been fitted to equation 5.5 The Q-dependence of the lidocaine EISF is shown in Figure

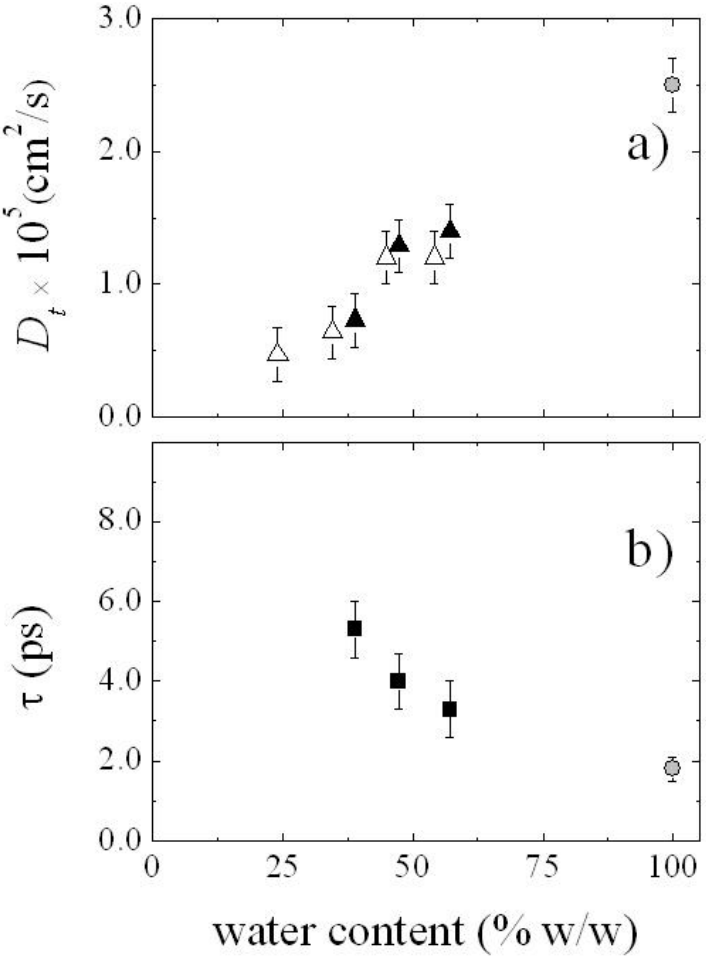

Figure 5.6: Hydration dependence of the microdiffusivity parameters of hydration water: a) self-diffusion coefficient, D_t, for samples in H_2O (full triangles) and in D_2O (open triangles); b) residence time between jumps, τ, for samples in H_2O (full squares). In both panels the gray circles indicate the values of D_t and τ for bulk water. Within the error bars, their values are consistent with literature ones [[52] and refs. therein].

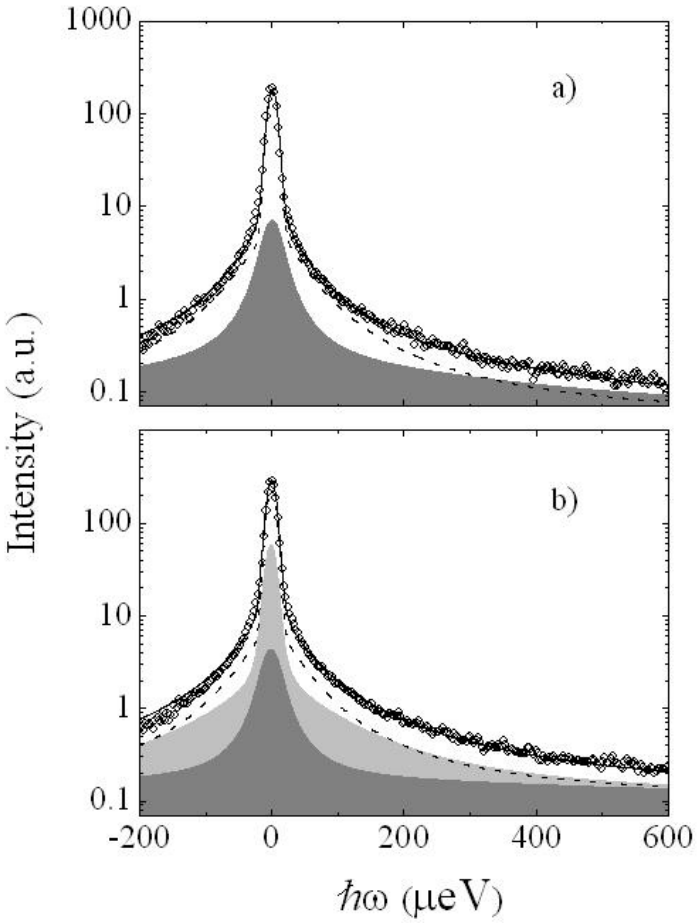

Figure 5.7: QENS spectra at Q = 0.44 Å^{-1} of a PD sample at h = 0.6 (a), and of a LD sample at h = 0.5 (b). The subspectra due to the polymer film (dashed lines) and to water (dark grey areas) are evidenced. In panel b) the subspectrum due to lidocaine is also indicated (light grey area). In both figures the logarithmic scale visually enhances the water contributions (dark grey): their areas are about 15 % of the total.

5.8 together with the fit according to equation 5.8:

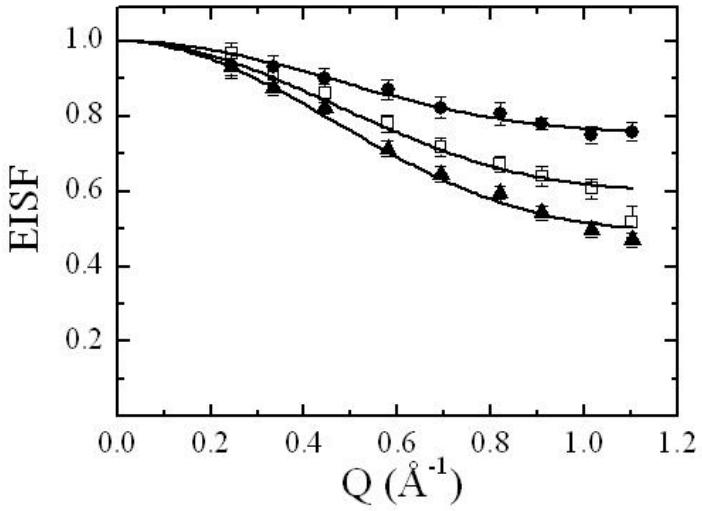

Figure 5.8: Q-dependence of the lidocaine EISF for LD samples at different hydrations: (h = 0.15 (black circles), 0.40 (open squares), 0.50 (black triangles)). The curves are fits to equation 5.8

The radius of confinement (r = 3.5 $\pm$ 0.6 Å) is almost hydration independent and the fraction of "immobile" protons, f, decreases from $\sim$ 0.8 at h = 0.15 to 0.4 at h = 0.6. This behavior is qualitatively similar to that of the polymer matrix. The width Γ_l of the quasielastic component describing the internal dynamics of lidocaine is almost Q-independent (average value 109 $\pm$ 3 μeV) as expected for local conformational motions. Upon increasing hydration above $h \sim 0.15$, the lidocaine subspectrum broadens indicating that lidocaine molecules diffuse through the hydrated matrix. This further motion is described as a Brownian process in equation 5.6 in terms of a Lorentzian function, $L_{diff}(Q,\omega)$, whose width scales linearly with Q^2 ($\Gamma_{diff} = D_t \cdot Q^2$). Here, D_t represents the diffusion coefficient of the lidocaine center of mass. The Q-dependence of $\Gamma_l + \Gamma_{diff}$ is shown in Figure 5.9:

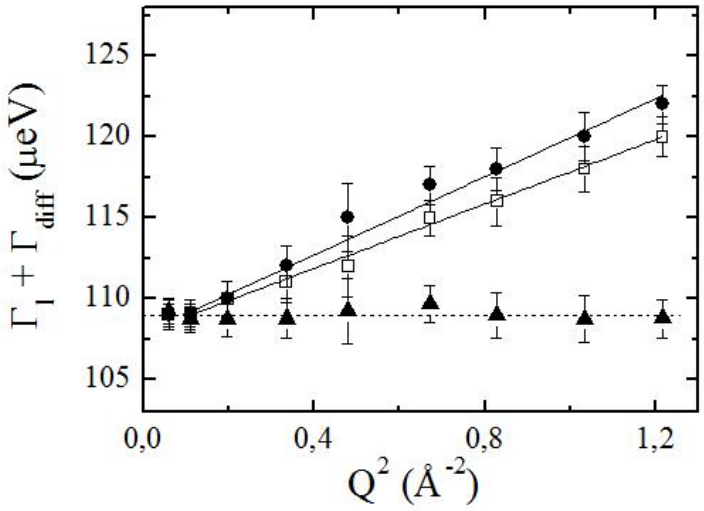

Figure 5.9: Q^2-dependence of the Lorentzian broadening, $\Gamma_l + \Gamma_{diff}$, obtained by the convolution of L_l and L_{diff} in equation 5.6. LD15 (black triangles), LD25 (open squares), LD50 (black circles). The continuous lines are linear fits to the data.

Up to h = 0.15, no long range diffusion is observed ($\Gamma_l + \Gamma_{diff}$ does not show any significant Q-dependence). At higher hydration, from the slopes of the lines in Figure 5.9, one can derive the translational diffusion coefficient, D_t, of lidocaine through the film. The obtained values are reported in Table 5.1: they are consistent with an estimate of lidocaine diffusivity in pure water ($D \sim 10^{-6}$ cm^2/s) that can be obtained using the Stokes-Einstein relation $D = k_B T/6\pi\eta r$ where k_B is the Boltzmann constant, T the absolute temperature, η the viscosity medium and r the hydrodynamic radius of the diffusing molecule.

Table 5.1: Translational diffusion coefficients of lidocaine within the film at different hydrations.

Sample	**D$_t$ lidocaine($\times 10^5$cm^2/s)**
LD25	0.15 ± 0.02
LD50	0.19 ± 0.01
LH40	0.18 ± 0.03
LH50	0.19 ± 0.01

5.4 Conclusions

Patch-non-Patch® films show a marked swelling upon water uptake, and macroscopic permeation measurements require a solid support, usually a porous membrane. In such experiments one therefore measures the diffusion through the membrane+film system which is largely determined by the diffusivity properties of the membrane. On the other hand microscopic techniques like QENS or pulse field gradient NMR provide a direct estimate of the drug diffusivity through the film without any additional

support. In the considered hydration range (up to 0.60) water plays a crucial role on the performance and behavior of the Patch-non-Patch® system. Concerning the dynamics of the polymer film, the main effect observed is an almost linear decrease with increasing hydration of the fraction of 'immobile' hydrogens as shown in Fig. 9a, while the distribution of relaxation times deduced from the width of the quasielastic spectrum and the volume explored by hydrogens in their confined motion, as deduced from the EISF, do not change appreciably. The different slopes in Fig. 9a between H_2O and D_2O solvents is due to the degree of H/D substitution of the exchangeable hydrogens in the film.

At low hydration levels $h < 0.15$ water molecules are closely bound to the polymer matrix and no long-range diffusion can take place. Upon increasing hydration the additional water molecules are 'mobile' and can diffuse through the matrix although with a reduced diffusivity with respect to bulk water. The diffusive dynamics of lidocaine is driven by the above behavior of water: Brownian diffusion within the patch is observed only when 'mobile' water is present ($h > 0.15$). Further increase of film hydration (up to $h \sim 0.6$) does not change appreciably the lidocaine diffusion coefficient which is about an order of magnitude lower than the self-diffusion coefficient of pure water. As concerns the intra-molecular dynamics of lidocaine, we observe that the relaxation time deduced from the width of the quasielastic spectrum and the radius of the confined diffusion sphere are not hydration sensitive, while the fraction f of non-diffusing hydrogens scales linearly with water content (Figure 5.10b). It is worth noticing that in this case no difference is observed between hydrogenous and deuterated buffer; this is not surprising since in the lidocaine molecule no exchangeable hydrogens are present. Overall, the results of the present work indicate that water controls and "triggers" the release properties of the drug through the Patch-non-Patch® system. The use of a microscopic

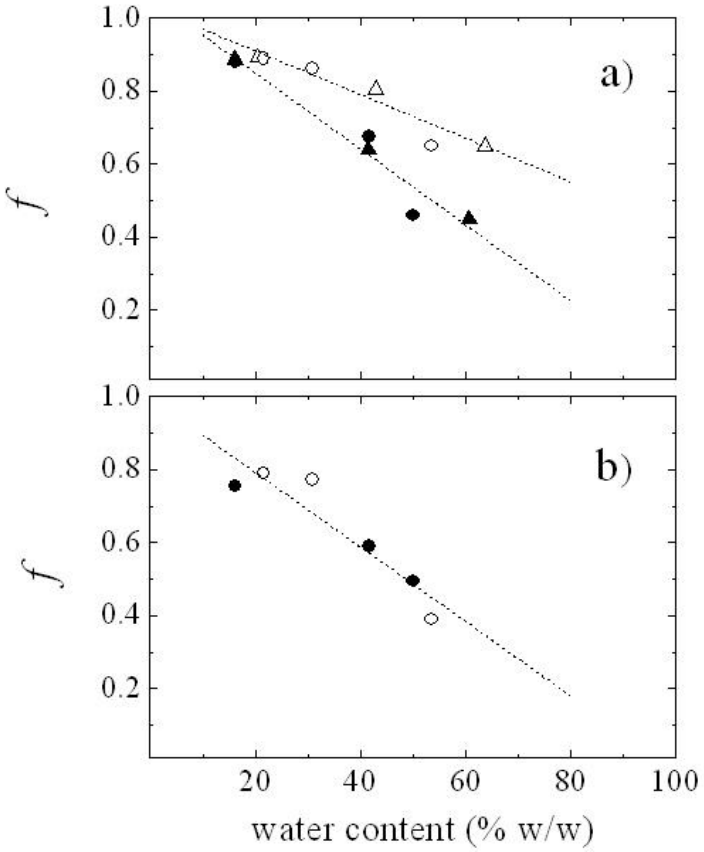

Figure 5.10: a) Fraction f of immobile hydrogens in the polymer film vs. water content. b) Same as in panel a) but in the case of the lidocaine molecule. Solid symbols refer to H_2O hydrated samples (PH (black triangles), LH(black circles)). Open symbols refers to D2O hydrated samples (PD (open triangles), LD (open circles)). The curves are linear fits to the data.

technique like QENS made it possible to obtain quantitative information on a complex system of direct pharmacological relevance.

Bibliography

[1] M. M. Smith, M. A. Cake, P. Ghosh, A. Schiavitano, R. A. Read, and C. B. Little. Significant synovial pathology in a meniscectomy model of osteoarthritis: modification by intra-articular hyaluronan therapy. *Rheumatology*, 47(8):1172–1178, August 2008.

[2] P. Colombo, P.L. Catellani, C. Padula, P. Santi, and G. Colombo. Film for dermal and transdermal administration of drugs, April 2002. International publication number WO 02/30402 A3.

[3] `http://patchnonpatch.awardspace.com`.

[4] C. Padula, S. Nicoli, V. Aversa, P. Colombo, F. Falson, F. Pirot, and P. Santi. Bioadhesive film for dermal and transdermal drug delivery. *Eur. J. Dermatol.*, 17(4):309–312, 2007.

[5] C. Padula, G. Colombo, S. Nicoli, P.L. Catellani, G. Massimo, and P Santi. Bioadhesive film for the transdermal delivery of lidocaine: in vitro and in vivo behavior. *J. Control Release*, 88(2):277, 2003.

[6] C. Padula, S. Nicoli, P. Colombo, and P. Santi. Single-layer transdermal film containing lidocaine: modulation of drug release. *Eur. J. Pharm. Biopharm.*, 66(3):422–428, 2007.

[7] M. Bée. *Quasi elastic neutron scattering*. Adam Hilger, 1988.

[8] L. Van Hove. Correlations in space and time and born approximation scattering in systems of interacting particles. *Phys. Rev.*, 95:249–262, 1954.

[9] R. Fieschi and R. De Renzi. *Struttura della Materia*. Carocci, 1995.

[10] D. Knorr. Novel approaches in food-processing technology: new technologies for preserving foods and modifying function. *Curr. Opin. Biotechnol.*, 10:485–491, 1999.

[11] P. Masson, C. Tonello, and C. Balny. High-pressure biotechnology in medicine and pharmaceutical science. *J. Biomed. Biotechnol.*, 1:85–88, 2001.

[12] K. Akasaka, T. Tezuka, and H. Yamada. Pressure-induced changes in the folded structure of lysozyme. *J. Mol. Biol.*, 271:671–678, 1997.

[13] A. Filabozzi, A. Deriu, M.T. Di Bari, D. Russo, S. Croci, and A. Di Venere. Elastic incoherent neutron scattering as a probe of high pressure induced changes in protein flexibility. *Biochimica et Biophysica Acta*, 1804:63–67, 2010.

[14] G. Tettamanti et al. *Physics of Amphiphiles: Micelles, Vescicles and Microemulsions*, page 607. North-Holland, Amsterdam, 1985.

[15] S. Sonnino, L. Cantù, M. Corti, D. Acquoti, and B. Venerando. Aggregative properties of gangliosides in solution. *Chem. Phys. Lipids*, 71:21–45, 1994.

[16] L. Jr. Lapcik, L. Lapcik, S. De Smedt, and J. Demeester. Hyaluronan: Preparation, structure, properties, and applications. *Chem. Rev.*, 98:2663–2684, 1998.

[17] T. C. Laurent. *The Chemistry, Biology and Medical Applications of Hyaluronan and its Derivatives*. Portland Press: London, 1998.

[18] A. Schiavinato and D. Bellini. Us 0069884 a1. Fidia Farmaceutici, S.p.A., 2008.

[19] K. S. Schmitz. *An Introduction to Dynamic Light Scattering by Macromolecules*. Academic Press: London, 1990.

[20] J. S. Higgins and H. C. Benoît. *Polymers and Neutron Scattering*. Oxford University Press Inc.: New York, 1994.

[21] F. Horkay, P. Bassera, A.-M. Hecht, and E. Geissler. Structural investigations of a neutralized polyelectrolyte gel and an associating neutral hydrogel. *Polymer*, 46:4242–4247, 2005.

[22] A.-M. Hecht, F. Horkay, and E. Geissler. Neutron scattering investigations on a bimodal polymer gel. *J. Phys. Chem. B*, 105(24):5637–5642, 2001.

[23] F. Horkay, G.B. McKenna, P. Deschamps, and E. Geissler. Neutron scattering properties of randomly cross-linked polyisoprene gels. *Macromolecules*, 33(14):5215–5220, 2000.

[24] P. Debye and R.M. Bueche. Scattering by an inhomogeneous solid. *J Appl Phys*, 20:518–, 1949.

[25] J. S. Pedersen and P. Schurtenberger. Scattering functions of semiflexible polymers with and without excluded volume effects. *Macromolecules*, 29:7602, 1996.

[26] `http://cerlib.web.cern.ch/cernlib/`.

[27] J. Teixeira, M.-C. Bellissent-Funel, S.-H. Chen, and A.J. Dianoux. Experimental determination of the nature of diffusive motions of water molecules at low temperatures. *Phys. Rev. A*, 31:1913–1917, 1985.

[28] F. Cavatorta, A. Deriu, D. Di Cola, and H.D. Middendorf. Diffusive properties of water studied by incoherent quasi-elastic neutron scattering. *J. Phys.: Condens. Matter*, 6:A113–A117, 1994.

[29] F. Volino and A.J. Dianoux. Neutron incoherent scattering law for diffusion in a potential of spherical symmetry: general formalism and application to diffusion within a sphere. *Mol. Phys.*, 41:271–279, 1980.

[30] P.A. Egelstaff. *An Introduction to the Liquid State*, pages 221–225. Oxford Science Publications, 1994.

[31] D. Di Cola, A. Deriu, M. Sampoli, and A. Torcini. Proton dynamics in supercooled water by molecular dynamics simulations and quasielastic neutron scattering. *J. Chem. Phys.*, 104:4223–4232, 1996.

[32] M.R. Harpham, B.M. Ladanyi, N.E. Levinger, and K.W. Herwig. The effect of the counterion on water mobility in reverse micelles studied by molecular dynamics simulations. *J. Chem. Phys.*, 121:7855–7868, 2004.

[33] L. Liu, A. Faraone, C. Mou, C.W. Yen, and S.H. Chen. Slow dynamics of supercooled water confined in nanoporous silica materials. *J.Phys.: Condens. Matter*, 16:S5403–S5436, 2004.

[34] V.F. Sears. Theory of cold neutron scattering by homonuclear diatomic liquids. *Can. J. Phys.*, 44:1299–1311, 1966.

[35] D. Laage and J.T. Hynes. A molecular jump mechanism of water reorientation. *Science*, 311:832–835, 2006.

[36] D. Laage and J.T. Hynes. On the molecular mechanism of water reorientation. *J. Phys. Chem. B*, 112:14230–14242, 2008.

[37] D. Laage. Reinterpretation of the liquid water quasi-elastic neutron scattering spectra based on a nondiffusive jump reorientation mechanism. *J. Phys. Chem. B Letters*, 113:2684–2687, 2009.

[38] M. Tehei, B. Franzetti, K. Wood, F. Gabel, E. Fabiani, M. Jasnin, et al. Neutron scattering reveals extremely slow cell water in a dead sea organism. *PNAS*, 104:766–771, 2006.

[39] E. Buhler and F. Boué. Chain persistence length and structure in hyaluronan solutions: Ionic strength dependence for a model semirigid polyelectrolyte. *Macromolecules*, 37:1600–1610, 2004.

[40] F. Horkay, A.-M. Hecht, C. Rochas, P. Basser, and E. Geissler. Anomalous small angle x-ray scattering determination of ion distribution around a polyelectrolyte biopolymer in salt solution. *J. Chem. Phys.*, 125:234904, 2006.

[41] J.A. Hornemann, A.A. Lysova, S.L. Codd, J.D. Seymour, S.C. Busse, P.S. Stewart, et al. Biopolymer and water dynamics in microbial biofilm extracellular polymeric substance. *Biomacromolecules*, 9:2322–2328, 2008.

[42] M.C. Hacker, A. Haesslein, H. Ueda, W.J. Foster, C.A. Garcia, D.M. Ammon, et al. Biodegradable fumarate-based drug-delivery systems for aphtalmic applications. *J. Biomed. Mater. Res. Part A*, 88A:976–989, 2009.

[43] M. Vogt, H.-C. Flemming, and W.S. Veeman. Diffusion in pseudomonas aeruginosa biofilms: a pulsed field gradient nmr study. *J. Biotechnol.*, 77:137–146, 2000.

[44] S. Nicoli, P. Colombo, and P. Santi. Release and permeation kinetics of caffeine from bioadhesive transdermal films. *AAPS Journal*, 7:E218–E223, 2005.

[45] A. Femenia-Font, C. Padula, F. Marra, C. Balaguer-Fernandez, V. Merino, A. Lopez-Castellano, et al. Bioadhesive monolayer film for the in vitro transdermal delivery of sumatriptan. *J. Pharm. Sci.*, 95:1561–1569, 2006.

[46] S. Nicoli, E. Penna, C. Padula, P. Colombo, and P. Santi. New transdermal bioadhesive film containing oxybutynin: in vitro permeation across rabbit ear skin. *Int. J. Pharm.*, 325:2–7, 2006.

[47] A. Nussinovitch, A. Gal, C. Padula, and P. Santi. Physical characterization of a new skin bioadhesive film. *AAPS Pharm. Sci. Tech.*, 9:458–463, 2008.

[48] A. Arbe, J. Colmenero, M. Monkenbusch, and D. Richter. Dynamics of glass-forming polymers: ”homogeneous” versus ”heterogeneous” scenario. *Phys. Rev. Lett.*, 81:590–593, 1998.

[49] P.S. Belton. Nmr and the mobility of water in polysaccharide gels. *Int. J. Biol. Macromol.*, 21:81–88, 1997.

[50] F. Cavatorta, N. Angelini, A. Deriu, and G. Albanese. Vibrational dynamics of hydration water in amylase. *Appl. Phys. A-Mater.*, 74:S504–S506, 2002.

[51] V. Calandrini, A. Deriu, G. Onori, R.E. Lechner, and J. Pieper. Diffusive dynamics of water in tert-butyl alcohol/water mixtures. *J. Chem. Phys.*, 120:4759–4767, 2004.

[52] M.T. Di Bari, Y. Gerelli, F. Sonvico, A. Deriu, F. Cavatorta, G. Albanese, and others. Dynamics of lipid-saccharide nanoparticles by quasielastic neutron scattering. *Chem. Phys.*, 345:239–244, 2008.